https://doi.org/10.5194/gmd-2023-48
Preprint. Discussion started: 29 March 2023

Geoscientific Model Development Discussions

Peatland-VU-NUCOM (PVN 1.0): Using dynamic PFTs to model peatland vegetation, CH4 and CO2 emissions

Tanya J.R. Lippmann[1], Monique M.P.D. Heijmans[2], Ype van der Velde[1], Han Dolman[3,4], Dimmie M.D. Hendriks[5], and Ko van Huissteden[1,6]

[1]Vrije Universiteit, Amsterdam, the Netherlands
[2]Wageningen University and Research, Wageningen, the Netherlands
[3]Royal Netherlands Institute for Sea Research, Texel, the Netherlands
[4]Netherlands Earth System Science Center, Utrecht, the Netherlands
[5]Deltares Research Institute, Utrecht, the Netherlands
[6]VOF Kytalyk Carbon Cycle Research, Epse, the Netherlands

Correspondence: Tanya J.R. Lippmann (t.j.r.lippmann@vu.nl)

Abstract. Despite covering only 3% of the planet's land surface, peatlands store 30% of the planet's terrestrial carbon. The potential to both emit and drawdown CO_2 and CH_4, means that peatlands have a complex and multifaceted relationship with the global climate system. The net GHG emissions from peatlands depends on many factors but primarily vegetation composition, ground water level and drainage, land management, and soil temperature. Many peatland models use surface water levels to estimate CH_4 exchange, neglecting to consider the efficiency of CH_4 transported to the atmosphere by vegetation.

To assess the impact of vegetation on the GHG fluxes of peatlands, we have developed a new model, Peatland-VU-NUCOM (PVN). The new PVN model has been built from two parent models, the Peatland-VU and NUCOM-BOG models. To represent dynamic vegetation, we have introduced plant functional types and competition, adapted from the NUCOM-BOG model, into the Peatland-VU model. The PVN model includes plant competition, CH_4 diffusion, ebullition, root, shoot, litter, exudate production, below-ground decomposition, and above-ground moss development, under changing water levels and climatic conditions. PVN is a site-specific peatland CH_4 and CO_2 emissions model, able to reproduce vegetation dynamics.

Here, we present the PVN model structure and explore the model's sensitivity to environmental input data and the introduction of the new vegetation-competition schemes. We evaluate the model against observed chamber data collected at two peatland sites in the Netherlands to show that the model is able to reproduce realistic plant biomass fractions, and daily CH_4 and CO_2 fluxes. We find that this plot-scale model is flexible and robust and suitable to be used to simulate vegetation dynamics and emissions of other peatland sites.

1 Introduction

Peatlands are the world's largest terrestrial carbon store. Despite covering only 3% of the planet's land surface, peatlands store 30% (644 GtC) of the planet's terrestrial carbon (Yu et al., 2010), equivalent to 60% of the atmospheric carbon pool. The present day global radiative effect of peatlands on the climate are estimated to be between -0.2 and -0.5 Wm^{-2} (i.e. a net cooling) (Frolking and Roulet, 2007), in comparison to a radiative forcing of +2.43 Wm^{-2} due to all anthropogenic greenhouse

https://doi.org/10.5194/gmd-2023-48
Preprint. Discussion started: 29 March 2023

Geoscientific Model Development Discussions

gases since pre-industrial times (WGI, 2021). Future changes to the climate will impact the carbon sequestration capacity of peatlands, however, the net effect of climate change on peatlands is not yet understood (Loisel et al., 2021). Research indicates that some peatlands will form a positive feedback (Dorrepaal et al., 2009), whist others will form a neutral (Saleska et al., 2002), or negative feedback to warming of the global climate system (Melillo et al., 2002; Lafleur et al., 2003) and the net effect of these complex responses is not yet known.

The net warming effect of peatlands on the global climate system, and whether peatlands function as a carbon source or sink, is dependent on the net emission of two of the most prevelant atmospheric greenhouse gases, CO_2 and CH_4. Peatlands are large natural sources of global atmospheric CH_4 (Spahni et al., 2011). Between 2005 and 2008 (Zuo and Xiao, 2021), natural CH_4 emissions contributed approximately 50% of total CH_4 emissions (Saunois et al., 2020). Natural CH_4 emissions, particularly wetlands, are the greatest source of uncertainty in the global methane budget (Saunois et al., 2020). There exists a need to better constrain this estimate, requiring a better understanding of small scale processes (Bridgham et al., 2013). In peatlands, CH_4 is produced by anaerobic microbial communities found in the soil layer and therefore, the water level height plays a critical role on the net CH_4 flux.

The potential to both emit and drawdown CO_2 and CH_4, means that peatlands have a complex and multifaceted relationship with the global climate system. The net GHG emissions from peatlands depends on many factors but primarily vegetation composition, land management, ground water level and drainage, and soil temperature (Dorrepaal et al., 2009; Tiemeyer et al., 2016). Rewetting drained peatlands is one strategy proposed to combat enhanced CO_2 emissions from peatlands but has been documented to both enhance and reduce GHG emissions (eg. Günther et al. (2020); Boonman et al. (2022)) with the majority of studies concluding that rewetting leads to enhanced CH_4 and net GHG emissions, sometimes persisting for decades (Harpenslager et al., 2015; Knox et al., 2015). Rewetting refers to the practice of re-raising surface water levels of drained peatlands (Knox et al., 2015). Field studies have shown that vegetation restoration in combination with rewetting may reduce GHG emissions (Graf and Rochefort, 2009; Abdalla et al., 2016; Mazzola et al., 2022). Vegetation impacts the net GHG emissions in peatlands by directly influencing the net primary production (photosynthesis minus plant respiration) and organic matter available for decomposition and indirectly, by influencing the substrates available for microbial metabolization in the soil column. *Sphagnum* is a primary contributor to the carbon sequestration in peatlands and decompose three times slower than most vascular plants (Graf and Rochefort, 2009). To understand the role of vegetation emissions' feedbacks during peatland restoration efforts, vegetation must thus be treated as a dynamic interactive element of the peatland ecosystem.

There is an urgent need to expand model development efforts to assess the role of vegetation on GHG emissions of peatlands, particularly for peatland restoration efforts. Many peatland carbon cycle models have been developed over the preceding decades and the Wetland and Wetland CH_4 Inter-comparison of Models Project (WETCHIMP) evaluated the ability of a variety of models to simulate large-scale wetland characteristics and corresponding CH_4 emissions (Melton et al., 2013; Wania et al., 2013). WETCHIMP showed that peatland modelling efforts have made significant advancements to simulate CH_4 fluxes by including CH_4 specific processes such as CH_4 plant transport and ebulition. However, many models still use CO_2 and surface water levels as indicators of CH_4 exchange (Metzger et al., 2015). There exist only two pre-existing models that simulate peatlands, dynamic vegetation and CO_2 & CH_4 cycling (i.e. PEATBOG (Wu et al., 2016) and LPJ-WHyMe (Wania et al.,

https://doi.org/10.5194/gmd-2023-48
Preprint. Discussion started: 29 March 2023


Geoscientific Model Development Discussions

2010)) thereby limiting the ability to assess model mechanistic processes. The functionality and scope of current models that simulate peatlands and include either dynamic or static vegetation are compared in Table Fig. S1.

Plants with common ecosystem functions or structures (Wullschleger et al., 2014) can be represented with common model algorithms or parameters in a vegetation model when grouped as Plant Functional Types (PFTs). Shifts in community composition lead to feedbacks between species and other environmental parameters such as soil moisture, bulk density, soil organic matter (SOM) content, gas conduit function, rate of growth, rate of decomposition, microbial mineralisation, aerobic decomposition (De Boeck et al., 2011). Dynamic (rather than static) PFTs simulate the inter-seasonal growing and dying of plants, that over a number of years lead to vegetation succession, and are critical to reliably assess the impacts of climate and environmental change on peatland ecosystems (Box et al., 2019). Plant growth, root exudation and decomposition of organic matter happen at rates that differ depending on the plant type (Dorrepaal et al., 2007). Ecosystem storage of carbon happens through CO_2 uptake by photosynthesis and the slow decomposition of plant matter, leaf and root detritus, and root exudates in the anaerobic zone, but the efficiency of these processes vary between species. Plant detritus and root exudate excretion play a critical role in the availability of carbonic compounds and these vary depending on plant type. It has been shown that dynamic plant representation is critical to reliably simulate vegetation-environmental feedbacks in models (Toet et al., 2006) and therefore, the inclusion of dynamic vegetation classes is critical to reliably estimate C, CO_2 and CH_4 emissions from peatlands (Li et al., 2016; Laine et al., 2022).

To assess the impact of dynamic vegetation classes on subsequent GHG fluxes in peatlands we develop a new model, Peatland-VU-NUCOM v1.0 (PVN). PVN incorporates features of NUCOM-BOG, an ecosystem competition plot-scale model (Heijmans and Berendse, 2008) into the Peatland-VU model framework, a peatland process-based plot-scale model (van Huissteden et al., 2006). The NUCOM-BOG model simulates vegetation competition, C, nutrient, and water cycling in undisturbed bog ecosystems under changing climates. The NUCOM-BOG model simulates a soil profile divided by the acrotelm-catotelm boundary where plant growth and decomposition is partitioned between plant organs. The Peatland-VU model simulates the CH_4 and CO_2 cycle within a column of peat soil with varying water level. The Peatland-VU model simulates CH_4 fluxes, gross primary productivity and CO_2 cycle whilst assuming a constant plant layer and does not include a nitrogen cycle. We evaluate the new PVN model using automated flux-chamber observations measured at two rewetted previously drained peatland sites in the Netherlands. The inclusion of dynamic vegetation classes provides a model that is capable of investigating the impact of plant restoration efforts on GHG emissions from peatlands. All three models (NUCOM, PeatlandVU, and PVN) depend heavily on calibration using (often limited) observational data and for this reason, we do not expect to reproduce observed CH_4 and CO_2 more accurately. However, the aim is to create a model that reproduces the effects of plant species composition, changes thereof over time, and land management on GHG emissions.

2 Materials and Methods

The PVN model describes the vegetation, C, water, CH_4 and CO_2 dynamics of a column of an above- and below-ground peatland ecosystem. This new model incorporates key features of the NUCOM-BOG model (Heijmans and Berendse, 2008)

https://doi.org/10.5194/gmd-2023-48
Preprint. Discussion started: 29 March 2023


Geoscientific Model Development Discussions
Open Access
EGU

on plant specific traits and plant competition of peatland ecosystems systems into the framework of the Peatland-VU model (van Huissteden et al., 2006). The key strengths of the Peatland-VU model are to simulate CO_2 and CH_4 emissions, and the decomposition and production of below-ground SOM pools. The CO_2 and CH_4 pools and processes of the new PVN model are shown in the model schematic in Fig. 1. Extensive descriptions of the original NUCOM and Peatland-VU models can be found in Heijmans and Berendse (2008) and van Huissteden et al. (2006); Mi et al. (2014), respectively.

2.1 Model overview

With the aim of developing a peatland model capable of reproducing the impacts dynamic PFTs have on CO_2 and CH_4 emissions in peatlands, the new PVN model incorporate features of the NUCOM-BOG model Heijmans and Berendse (2008) into the framework of the Peatland-VU model van Huissteden et al. (2006); Mi et al. (2014). The new PVN model describes the vegetation, CH_4 and CO_2 dynamics of a column of an above- and below-ground peatland ecosystem. Carbon dioxide and CH_4 emissions enter the atmosphere by ebullition, transport through plants, diffusion through the soil, and respiration. The PVN model computes and simulates processes on a daily time step, as does the Peatland-VU model. Prior to this version of the model, the Peatland-VU model simulations were up to seven years in duration (Mi et al., 2014). The NUCOM-BOG model simulates vegetation succession and carbon balance over multi centennial timescales. We compare the new PVN model against the Peatland-VU model using multi decadal model simulation results. The Peatland-VU model is driven by daily air temperature (T), water level (WL), radiation, a soil parameter input file, and a general model parameter input file. The new PVN model has the same input requirements as the Peatland-VU model but now also requires input parameters for each PFT, discussed in 2.2 and 2.4.1.

2.2 Dynamic Plant Functional Types

Plant Functional Types (PFT) are the key element of NUCOM that is added to the Peatland-VU framework to create the PVN model. Any number of PFTs can be included in the model simulation. In this study we limit our simulations to six PFTs (*Typha*, sedges, tall grasses, short grasses, *Sphagnum*, and brown mosses) based on the vegetation communities observed at our test sites. Extensive descriptions of these PFTs are described in 2.4.1. PFT attributes (parameters) describe plant physiology, plant dynamics or bioclimatic limits. Each PFT has prescribed favourable temperatures and water levels for growth. Each PFT is prescribed as having either evergreen or deciduous phenology. For deciduous vegetation, leaf senescence occurs when daily temperatures fall below minimum tolerated temperatures. Maximum leaf coverage is maintained as long as daily water level and temperature are within the ideal threshold. The PFT parameters are defined in Table 1 and the values and references are listed in Table 2 and Table S2, respectively. Model processes calculated per PFT are represented using a 'p' in the model equations.

https://doi.org/10.5194/gmd-2023-48
Preprint. Discussion started: 29 March 2023

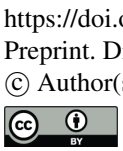

Geoscientific Model Development Discussions
Open Access
EGU

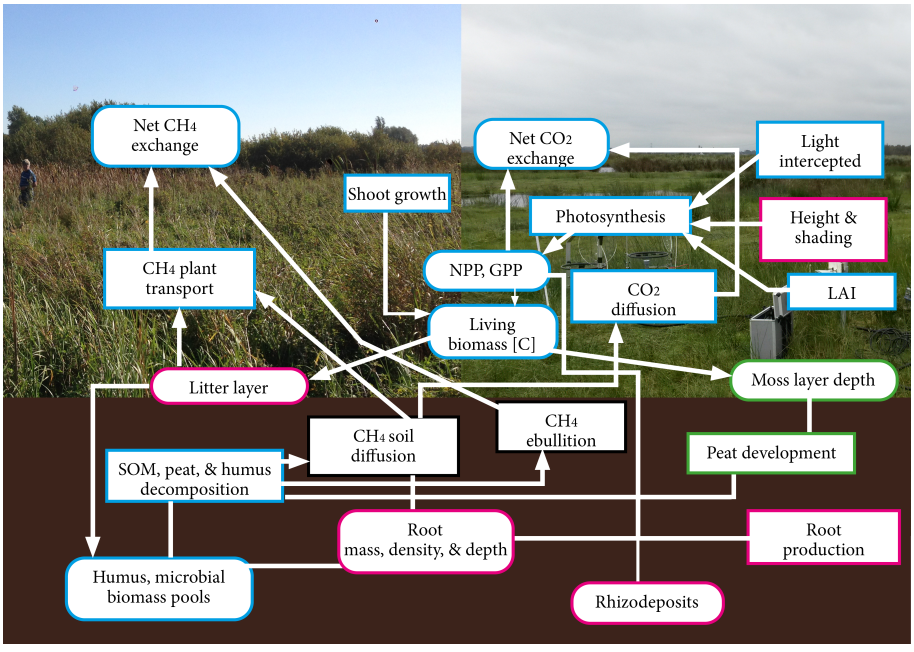

Figure 1. Schematic of the production, consumption and transport of carbon in the model. Dynamics and processes are delineated with rectangles, whereas carbon pools are delineated with curved edges. The pink outline represents non-moss pools and processes, green outline represents pools and processes applicable only to moss PFTs and the blue outline refers to pools and processes that are applicable for all plant types.

2.2.1 PFT carbon pools and initialisation

The below-ground carbon pools are peat, labile organic matter, exudates, microbial biomass, litter & dead roots, and root exudates. The above-ground carbon pools are living biomass, litter layer (non-moss PFTs only), shoots, and living moss depth (moss PFTs only) are initialised. The model generates a soil horizon representation using soil layers of equal thicknesses. The generated soil horizon uses properties such as DBD, SOM ratio, clay & sand content, C:N ratio specified in the soil profile. The number, depth, and thickness of the site's soil horizons can be adjusted in the soil input file. Following the development of the model's soil horizon, the root density, root distribution, and root mass of each PFT is mapped to the layout of the model's soil horizon representation (depth, density, layer thickness). To account for differences in decomposition rates among roots, and exudates, each PFT has designated SOM pools, which are partitioned between the soil layers. Root distribution, and root mass decrease exponentially from the surface to the PFT maximum root depth. In this section, the subscript p is used to show that the equation or variable is PFT specific, z to indicate that the equation or variable is soil layer specific, and the subscript t to represent time.

Biomass fraction (BF) is a representation of the ratio of PFT biomass to total biomass (Eq. 1). The sum of all PFTs are constrained to a maximum BF of 1.0. All PFTs have a minimum BF of 0.1 and are able to further establish when the conditions

https://doi.org/10.5194/gmd-2023-48
Preprint. Discussion started: 29 March 2023

Geoscientific Model Development Discussions
Open Access
EGU

Table 1. List and description of the PFT input parameters. The values assigned to each PFT are listed in Table 2. Associated references are listed in Table S2. In the left column each PFT parameter is tied to its relevant model mechanism. Note that some PFT parameters are, at times, used by multiple model processes.

Corresponding model process	Parameter	Description
Above-ground biomass	BiomassSenescence	Fraction of above-ground biomass littered each day
	AutumnLitter	For deciduous plants, fraction of leafy biomass littered each day during autumn
	CBiomassRatio	C to biomass ratio
	ShootsFactor	Mass fraction of primary production that consists of shoots; the remainder is root growth
	MaxCanopyHeight	Maximum height
Photosynthesis & respiration	PlantResp0	Plant respiration at zero degrees
	Temp_MaxPhoto	Maximum temperature limit for photosynthesis
	Temp_MinPhoto	Minimum temperature limit for photosynthesis
	TMinGrowth	Minimum temperature for growth
	TOptMinGrowth	Lowest temperature for optimal growth
	TOptMaxGrowth	Highest temperature for optimal growth
	TMaxGrowth	Maximum temperature for growth
	LeafRespirationCoeff	Leaf maintenance respiration coefficient
	MaxGrowthRate	Maximum growth rate
LAI	SpecificLeafArea	Ratio of leaf area to dry leaf mass
	MinLAI	Minimum LAI
	MaxLAI	Maximum LAI
	LightExtCoeff	Light extinction coefficient
CH_4 scheme	MethanePlantOx	Fraction of CH_4 that is oxidized during plant transport
	MethanePType	Vegetation type factor for gas transport through plant.
Roots, exudates	MaxRootDepth	Maximum root depth
	RootSenescence	Proportion of root mass that dies during each time step
	ExudateFactor	Mass fraction of of below-ground production that consists of exudates
	SpringCorrection	Coefficient for stronger exudation in spring
Below-ground decomposition	LitterConversion	Conversion factor of above-ground to below-ground litter; the factor is temperature adjusted such that at 0 degrees the conversion factor is also 0
	ResistFrac	Fraction of decomposed organic material that is transferred to resistant humus fraction
	AssimDissim	The amount of C from decomposed organic matter converted to microbial biomass
Water level	WLMin	Minimum water level for growth
	WLOptMin	Lowest water level for optimal growth
	WLOptMax	Highest water level for optimal growth
	WLMax	Maximum water level for growth

become favourable, as adapted from the NUCOM-BOG model.

$$BF_{t,p} = \frac{CB_{t,p}}{\sum_{p=1}^{P}(CB_{t,p})} \quad (1)$$

https://doi.org/10.5194/gmd-2023-48
Preprint. Discussion started: 29 March 2023

where, CB = biomass [kg C m^{-2}], t refers to time, and p refers to PFT.

2.2.2 Competition among PFTs

Each plant competes for light where taller PFTs have monopoly over shorter PFTs. Light that is not intercepted by the tallest PFT, becomes available to the next PFT, in descending height order. Light which is not intercepted by the non-moss PFTs is passed on and divided between moss PFTs, proportional to their BF. In this way, an increase (decrease) of foliage of taller PFTs may reduce (increase) the growth rates of mosses due to shading by limiting light exposure. At the beginning of each model day, non-moss PFTs are ordered according to descending height so that the shading by taller PFTs impacts the amount of light available to shorter PFTs. Plant height [m] is calculated using an allometric relationship adapted from Huang et al. (1992); Smith et al. (2001) (Eq. 2 and Eq. 3):

$$H_{t,p} = k_1 \cdot D_{t,p}^{k_2} \tag{2}$$

where,

$$D_{t,p} = \left(\frac{4 \cdot CB_{t,p}}{BD \cdot \pi \cdot k_2} \right)^{\frac{1}{2+k_3}} \tag{3}$$

where, BD represents biomass density [kg C m^{-3}], k_1 [m], k_2 [-], and k_3 [-] in Eq. 2 and Eq. 3 are constants with values 1, 40, and 0.85, taken from Smith et al. (2001). The light absorbed ($FPAR$, Eq. 4) by each PFT is dependent on the amount of shading from taller plants and their LAI.

$$FPAR_{t,non-moss} = (1 - e^{-LEC_p}) \cdot CB_{t,p} \cdot SLA_p \tag{4}$$

Where, LEC represents the Light Extinction Coefficient parameter [-], and SLA represents the Specific Leaf Area [m^2 kg^{-1} C]. The growth of the above-ground living biomass (Eq. 5) is dependent on shoot growth and biomass senescence lost to the litter layer.

$$\frac{\delta}{\delta t} CB_{t,p} = SM_{t,p} - BS_{t,p} \tag{5}$$

where, CB represents above-ground living biomass [kg C m^{-2}], SM represents shoot mass [kg C m^{-2}], calculated using Eq. 6, and $BS_{t,p}$ represents the fraction of above-ground biomass littered each day [day^{-1}].

$$SM_{t,p} = RS_p \cdot NPP_{t,p} \tag{6}$$

where, NPP represents the Net Primary Productivity [kg C m^{-2}] and RS represents the ratio of shoot to root growth. If the harvest scheme is activated, as prescribed in the model input files, PFTs taller than the prescribed height are harvested.

https://doi.org/10.5194/gmd-2023-48
Preprint. Discussion started: 29 March 2023


Geoscientific Model Development Discussions
Open Access
EGU

The harvest height and days are optional prescribed model parameters. Living biomass decreases according to the amount of biomass harvested (or mowed), under the assumption that biomass is uniformly distributed with height. A fixed percentage of the harvested material remains uncollected in the field and is added to the litter layer. LAI [m^2 m^{-2}] is calculated (Eq. 7) as a function of living biomass, the water growth factor (WG) and SLA, whilst constrained by prescribed minimum and maximum LAI values.

$$LAI_{t,p} = \frac{CB_{t,p} \cdot SLA_p}{(LEC_p \cdot \frac{\delta}{\delta t} LAI_{t,p} + (1 - e^{-WG_{t,p}}))} \tag{7}$$

where WG refers to the water growth function (Eq. 12 [-]). Growth of individual moss PFTs (HG, Eq. 8) is represented in terms of fractional cover, rather than height. A moss PFT with more cover has access to more light and gains an advantage over other mosses. Moss PFTs grow at different rates due to differences in the range of temperatures, and water levels they can grow. The depth (or thickness, [m]) of both individual moss PFTs (Eq. 8), and the total living moss layer (Eq. 9) are dependent on BF, potential growth , and dry bulk density (DBD, kg C m^{-3}).

$$HG_{t,p} = \frac{PG_{t,p} \cdot BF_{t,p}}{DBD_{t,p,z=1}} \tag{8}$$

The moss thicknesses of individual moss PFTs are aggregated to calculate the total ecosystem moss depth (MHG):

$$MHG = \frac{SHG_{t,p}}{\sum_{p=1}^{P} BF_{t,p}} \tag{9}$$

where,

$$SHG_{t,p} = \sum_{p=1}^{P} (HG_{t,p} \cdot BF_{t,p}) \tag{10}$$

The WG and TG functions impact the development of moss PFTs by impacting the potential growth. Potential growth, WG, and TG are adapted functions from Heijmans and Berendse (2008). Potential Growth (PG [-], Eq. 11) reflects the favourability of water levels or temperatures:

$$PG_{t,p} = FPAR_{p,t} \cdot Gmax_p \cdot TG_{T,t,p} \cdot WG_{W,t,p} \tag{11}$$

https://doi.org/10.5194/gmd-2023-48
Preprint. Discussion started: 29 March 2023

Geoscientific Model Development Discussions

The WG and TG functions (unitless) are congruent to each other and therefore we have only written out the WG function:

$$\begin{aligned} WG_{p,t} \\ &= 0, \text{ if } WL < WL_{min} \\ &= \frac{WL - WL_{min}}{WL_{minopt} - WL_{min}}, \text{ if } WL_{min} < WL < WL_{minopt} \\ &= 1, \text{ if } WL_{minopt} < WL < WL_{maxopt} \\ &= \frac{WL_{max} - WL}{WL_{max} - WL_{maxopt}}, \text{ if } WL_{maxopt} < WL < WL_{max} \end{aligned} \tag{12}$$

where, WL = water level, min (max) = minimum (maximum) tolerated water level, and $minopt$ ($maxopt$) = minimum (maximum) optimum water level.

2.3 CH_4 processes

The net CH_4 flux (Eq. 13) is the sum of plant transported CH_4 (Qpl, Eq. 14) and the below-ground processes: anaerobic CH_4 production (Rpr), CH_4 oxidation (Rox), ebullition (Qeb), and diffusion of CH_4 through soil ($Fdiff$). The soil layer is subdivided into 15 layers of equal thickness (0.1 m) and the flux rate of each layer is calculated before integrating over all layers to obtain the total CH_4 flux. These CH_4 process were adapted from the Peatland-VU model described in Mi et al. (2014); van Huissteden et al. (2006).

$$\frac{\delta}{\delta t} C_{CH_4,t,z} = \sum_{p=1}^{P} (Qpl_{t,p,z}) - \frac{\delta}{\delta Z} Fdiff_{t,z} + Qeb_{t,z} + Rpr_{t,z} + Rox_{t,z} \tag{13}$$

Where C_{CH_4} represents the CH_4 concentration [μM m^{-3}] at time, t and depth z, Qpl [μM m^{-3} day^{-1}] is the CH_4 flux by plant roots, $Fdiff$ [μM m^{-2} day^{-1}] is the diffusive flux. Qeb [μM m^{-3} day^{-1}] represents ebullition of CH_4, Rpr [μM m^{-3} day^{-1}] is the production of CH_4 by anaerobic peat oxidation, and Rox [μM m^{-3} day^{-1}] is the removal of CH_4 by oxidation of CH_4 to CO_2 in the soil.

The PVN model has adapted the plant transport pathway so that plant transported CH_4 is calculated for each PFT. Anaerobic CH_4 production, ebullition and diffusion of CH_4 through the soil remain as described in Mi et al. (2014); van Huissteden et al. (2006), originally adapted from Walter et al. (2001). There are two mechanisms which determine the amount of CH_4 lost via plant transport. Firstly, the spread and density of the root system plays a role in determining how much CH_4 is taken up into the plant tissue. Thereby, a dense or large root system enables, along with enhanced soil CH_4 concentrations, more CH_4 to enter the plant tissue. Secondly, the amount of CH_4 transported through the plant tissue and released to the atmosphere is determined by its aerenchyma. Plants with (without) large aerenchyma are (in)efficient transporters of CH_4. The unitless parameter MethanePlantOx_PFT ($PlOx$ in Eq. 15) is used to delineate the plant's capacity to conduit CH_4.

$$Qpl_{t,p,z} = -cP \cdot vP_p \cdot LAI_{t,p} \cdot RD_{t,p,z} \cdot C_{CH_4,t,z} \tag{14}$$

https://doi.org/10.5194/gmd-2023-48
Preprint. Discussion started: 29 March 2023

Geoscientific Model Development Discussions

where, RD is a function representing the distribution of roots per soil layer [-], cP represents the site specific CH_4 constant [day^{-1}] and vP represents the unitless PFT CH_4 rate constant, MethanePType_PFT. The rate of plant transported CH_4 is integrated over the depth of the root zone to obtain the flux at the surface(Eq. 15).

$$Fpl_{t,p,z} = \int_{z}^{0} \left[Qpl_{t,p,z} \cdot (1 - PlOx_p) \right] dz \tag{15}$$

where, Fpl represents the total plant transported CH_4 flux [μM day^{-1}].

2.3.1 CO_2 processes

At the beginning of each day, C3 photosynthesis (Eq. 19), leaf respiration (RE), and net primary production (NPP) are calculated using modified versions of the primary production scheme introduced in Mi et al. (2014), modified from Haxeltine et al. (1996). The net CO_2 fluxes for each PFT (NEE, Eq. 16) are the sum of photosynthesis minus plant respiration, the production of CO_2 by below-ground aerobic decomposition of inert SOM (KCO_2, [kg C m^{-2}]), and the portion of CO_2 oxidised from CH_4 (Rox).

$$NEE_{t,p} = AP_{t,p} + \int_{z}^{0} B_{CO_{2,t,p}} dz - \int_{z}^{0} RT_{t,p} dz \tag{16}$$

where, NEE is the Net Ecosystem Exchange [kg C m^2], AP is the daily potential photosynthesis calculated in Eq. 17 [kg C m^{-2}], B_{CO_2} is the CO_2 flux produced by below-ground SOM decomposition [kg C m^{-3}] (Eq. 22), and $RT_{t,p}$ is the daily plant respiration [kg C m^{-2}].

$$AP_{t,p} = FPAR_{t,p} \cdot \sigma \cdot \phi \cdot PAR \cdot AI_{t,p} \cdot fG_{t,p} \tag{17}$$

where $FPAR$ is the fraction of incoming PAR [J m^{-2} day^{-1}] absorbed by vegetation (Eq. 4), AI represents total daily incident PAR [gC m^{-2} day^{-1}], ϕ is the quantum efficiency of gross photosynthesis at prescribed ambient CO_2 [M-C M-photons^{-1}], fG is a unitless temperature stress scalar dependent on favourable air temperatures and incoming solar radiation, σ is a dimensionless factor that depends on the fractional day length (TD):

$$\sigma = \sqrt{1 - \frac{a_{t,p}}{TD_t}} \tag{18}$$

https://doi.org/10.5194/gmd-2023-48
Preprint. Discussion started: 29 March 2023

Geoscientific Model Development Discussions

where, a, the ratio of leaf respiration to photosynthetic capacity (we used the ratio value, 0.08, taken from Haxeltine et al. (1996)). Instantaneous photosynthesis (AI) is calculated by:

$$AI_{t,p} = \frac{\phi \cdot I \cdot A_{max,t,p}}{\phi \cdot I_{t,p} + A_{max,t,p}} - RE_{t,p} \tag{19}$$

where, I is the instantaneous PAR flux [J m^{-2} s^{-1}], A_{max} is the maximum rate of photosynthesis [J m^{-2} s^{-1}], and RE is the instantaneous rate of leaf respiration [g C m^{-2} s^{-1}].

$$RE_{t,p} = R_p * fG_{t,p} \tag{20}$$

where, where, fG is a unitless temperature stress scalar dependent on favourable air temperatures and incoming solar radiation, and R is the leaf respiration constant [g C m^{-2} s^{-1}].

2.3.2 Below-ground SOM decomposition

Each below-ground SOM pool (peat, labile organic matter, exudates, microbial biomass, litter & dead roots, root exudates) is partitioned between active and inert carbon pools, where the active carbon pool is available for microbial decomposition and then partitioned between CO_2 and CH_4. Non-moss PFTs do not contribute to the storage of peat. The decomposition of soil layers that lie beneath the water level are calculated, assuming first order rate kinetics:

$$\frac{\delta Q_{t,p,z}}{\delta t} = -k_p \cdot Q_{t,p,z} \tag{21}$$

where, Q is the mass of organic C in each SOM pool [kg C m^{-3}], and k is the decomposition rate [day^{-1}] for each SOM pool. The CO_2 flux from each SOM pool is calculated as:

$$B_{CO_2,t,p,z} = \frac{\delta Q_{t,p,z}}{\delta t} \cdot (1 - MI_{t,p,z} - HU_{t,p,z}) \tag{22}$$

where, MI [kg C m^{-2}] refers to SOM transferred to the microbial biomass pool and HU [kg C m^{-2}] refers to the SOM transferred to the resistant humus pool. The remaining fraction of $\frac{\delta Q_{t,p,z}}{\delta t}$ is transferred into CO_2.

2.3.3 Below-ground production

Root exudation plays an important role in the rhizosphere by promoting methanogensis and soil carbon loss through CH_4 production. The production of new roots (Rd) is based on a PFT prescribed shoot to root growth ratio and NEE. Root exudates (RX, Eq. 24) are a fraction of calculated below-ground root production ($Rd_{p,z,t}$). Exudates develop at a prescribed rate per PFT which is dependent on root and shoot growth.

$$\frac{\delta}{\delta t} RM_{t,p,z} = Rd_{t,p,z} - RX_{t,p} - RDR_{t,p} \tag{23}$$

https://doi.org/10.5194/gmd-2023-48
Preprint. Discussion started: 29 March 2023


Geoscientific Model Development Discussions

where, RM is the root mass [kg C m^{-2}] at time t, and soil depth z. Rd represents the growth of new roots [kg C m^{-2} day^{-1}], RDR represents the amount of death of existing roots [kg C m^{-2} day^{-1}].

$$RX_{t,p,z} = Rd_{t,p,z} \cdot FSP_{p,DoY} \cdot REX_{t,p} \tag{24}$$

where, DoY represents the Julian day of the year, REX represents the unitless root exudation factor so that maximum exudates occurs during spring ($FSP_{p,DoY}$).

$$RDR_{t,p,z} = RM_{t,p,z} \cdot RSX_p \tag{25}$$

where RSX represents the root senescence rate [day^{-1}].

$$Rd_{t,p,z} = \frac{\delta}{\delta t} RM_{t,p,z} \cdot NPP_{t,p} \cdot (1 - RS_p) \tag{26}$$

where, RS is a PFT shoot to root growth ratio [-].

2.3.4 Litter layer production and decomposition

Senescence of the above-ground living biomass is added to the litter layer, for non-moss PFTs. Senescence of moss PFTs contributes directly to the below-ground SOM pools:

$$\frac{\delta}{\delta t} LL_{t,p} = (1 - KB_p) \cdot CB_{t,p} - \frac{KL_p}{KT} \cdot T_t \tag{27}$$

where, leaf senescence, KB_p [day^{-1}], is set to 0.05 during Autumn, KL_p represents the fraction of leafy biomass littered during Autumn [day^{-1}], KT is the reference temperature [°C] and T represents daily air temperature [°C].

All model code has been written in C++. The model code is publicly available from the Bitbucket repository (bitbucket.org/tlippmann/pvn_public, last accessed 10 January 2023) under the GNU General Public License version 3, or any later version. Users are welcome to contact the authors for technical support. The model schematic in Fig. 1 was composed in Adobe Indesign. All other figures in this manuscript were plotted using Python and particularly the pandas, Seaborn and Matplotlib libraries.

2.4 Two peatland sites

With this study, the PVN model simulates two peatland sites in the Netherlands. The Ilperveld site (52°26' N, 4°56' E; 1.42 meters below sea level (mbsl)) is currently a nature recreation area that is a former raised bog complex that was drained to be used as agricultural pasture, and frequently exposed to manure fertilisation (van Geel et al., 1983; Harpenslager et al., 2015). Since the early 2000's, the Ilperveld site has undergone restoration efforts which included raising the water level, removal of the fertilised & nutrient rich top soil, attempts to re-introduce *Sphagnum*, and water quality management. The vegetation consists of

https://doi.org/10.5194/gmd-2023-48
Preprint. Discussion started: 29 March 2023


Geoscientific Model Development Discussions

brown mosses, *Sphagnum*, and grasses (*Poaceae* family). Since restoration began, the site has been mown twice a year, in June and September. Vegetation profiles show layers of intact *SphagnumCarex* peat and unlike undisturbed peatlands, the top layer has undergone greater decomposition due to land management since drainage (Harpenslager et al., 2015). The Horstermeer site (52°15' N, 5°04' E; 2.1 mbsl) lies on the Horstermeer polder and is a former drained agricultural peat meadow that has not been used since the 1990s when the water level was also raised. It was used for grazing and exposed to manure fertilisation until the 1990s. The Horstermeer site is now a semi-natural fen containing very heterogeneous vegetation, including reeds, grasses, and small shrubs, and is not subject to mowing or other land management practices (Hendriks et al., 2007). Vegetation consists of different types of grasses and sedges (dominant species *Holcus lanatus*, *Phalaris arundinacea*, *Glyceria fluitans*), and reeds (*Phragmites australis*, *Typha latifolia*). The Horstermeer polder is subject to strong seepage of mineral rich groundwater from surrounding lake areas and Pleistocene ice pushed ridges (Hendriks et al., 2007). The Horstermeer polder was a freshwater lake that was drained as part of large-scale land reclamation project completed in 1888.

2.4.1 PFT attributes

This study defined six PFTs (*Typha*, sedges, tall grasses, short grasses, *Sphagnum*, brown mosses) based on the vegetation communities observed at the Horstermeer and Ilperveld sites. PFT attributes (Table 2) were amalgamated from the NUCOM-BOG model, the TRY 5.0 database (https://www.try-db.org, last accessed 18 May 2022) (Kattge et al., 2011, 2020) and other relevant publications listed in Table S2. Sedges, tall grasses and *Typha* all represent graminoids with deep root systems that can grow at a range of water levels but have different aerenchyma and growing ranges. Sedges are from the family *Cyperaceae* and *Juncaceae* and are grass-like, monocotyledonous flowering plants with aerenchymae. Tall grasses are from the family *Poaceae* and are grass-like plants with elongated long blade-like leaves without aerenchyma. *Typha* PFTs represent a genus of about 30 species of monocotyledonous flowering plants in the family *Typhacea* with large aerenchyma. The short grasses PFT is representative of forbs and agricultural-like grasses with shallow root systems. The *Sphagnum* PFT is representative of hummock *Sphagnum* species which are generally more drought tolerant. Brown mosses represent all non-*Sphagnum* mosses but have similar but slightly broader temperature growth ranges. The SOM evolved from short grasses decomposes more easily than SOM evolved from brown mosses which decomposes more easily than SOM evolved from *Sphagnum*. The six PFT input parameters used in this study are accessible from the bitbucket repository, bitbucket.org/tlippmann/pvn_public.

2.4.2 Model calibration

The model was calibrated to reproduce fluxes that fall within the spread of observed in situ chamber measurements, measured at the Horstermeer and Ilperveld peatland sites (described in Sect. 2.4). A Monte Carlo analysis was performed separately for each site to calibrate the model input parameters. Since the CO_2 results impact the CH_4 results much more than the CH_4 results impact the CO_2 results, we first ensured that the parameters impacting the photosynthesis, and above and below ground growth and respiration schemes reproduced fluxes that fell within the spread of observed CO_2 fluxes (NEE). Next, the CH_4 scheme was calibrated to reproduce fluxes that fell within the spread of observed CH_4 fluxes. Even though the amount of photosynthesis and

https://doi.org/10.5194/gmd-2023-48
Preprint. Discussion started: 29 March 2023

Geoscientific Model Development Discussions

Table 2. Plant functional type parameters and bioclimatic limits. The parameter definitions are listed in 1. Associated references are listed in S2.

Parameter	Units	Tall grass	Sedges	*Typha*	*Sphagnum*	Brown moss	Short grass
BiomassSenescence	-	0.04	0.04	0.04	0.01	0.015	0.03
AutumnLitter	-	0.1	0.1	0.1	0.01	0.04	0.06
CBiomassRatio	$\mathrm{kgC\,kgC^{-1}}$	0.46	0.46	0.46	0.44	0.44	0.44
ShootsFactor	-	0.7	0.7	0.7	1.0	1.0	0.9
MaxCanopyHeight	m	1.5813	2.5813	2.5813	0.1	0.2	0.2
Temp_MaxPhoto	°C	38	40	35	30.0	30.0	30
Temp_MinPhoto	°C	-3	-1	-3	-1.0	0.5	-1
TMinGrowth	°C	7	2	2	-1.0	0.5	0.5
TOptMinGrowth	°C	9	12	12	14.0	5.0	14
TOptMaxGrowth	°C	20	30	30	25.0	25.0	25
TMaxGrowth	°C	45	45	45	38.0	38.0	38
LeafRespirationCoeff	-	0.015	0.015	0.015	0.016	0.014	0.014
MaxGrowthRate	$\mathrm{gC\,day^{-1}}$	0.07	0.07	0.07	0.045	0.05	0.05
SpecificLeafArea	$\mathrm{m^2\,g^{-1}}$	0.012	0.012	0.012	0.02	0.02	0.02
MinLAI	$\mathrm{m^2\,m^{-2}}$	0.1	0.1	0.1	0.1	0.1	0.1
MaxLAI	$\mathrm{m^2\,m^{-2}}$	3	4	4	1.2	1.5	1.5
LightExtCoeff	-	0.5	0.46	0.5	0.95	0.95	0.95
MethanePlantOx	-	0.4	0.4	0.25	0.7	0.8	0.6
MethanePType	-	5	6	10	2.0	2.0	2
MaxRootDepth	m	0.46	1	1	0.1	0.1	0.2
RootSenescence	$\mathrm{day^{-1}}$	0.05	0.05	0.05	0.04	0.04	0.05
ExudateFactor	-	0.1	0.2	0.2	0.05	0.1	0.11
SpringCorrection	-	0.2	0.4	0.4	0.0	0.0	0.1
LitterConversion	$\mathrm{day^{-1}}$	0.005	0.001	0.001	0.01	0.005	0.003
ResistFrac	-	0.55	0.42	0.3	0.9	0.9	0.9
AssimDissim	-	2.25	2.2	2.2	2.4	2.3	2.3
WLMin	m	-1	-1	-1	-0.5	-0.35	-0.35
WLOptMin	m	-0.4	-0.3	-0.4	-0.2	-0.15	-0.15
WLOptMax	m	-0.2	-0.2	0	-0.05	-0.05	-0.05
WLMax	m	0.0192	0.1	0.3	0.05	0.05	0.05

living biomass does not directly impact the CH_4 production, which primarily occurs in the soil and above-ground litter layers, these processes are precursors to root and shoot growth, respiration, and senescence, which directly impact simulated CH_4 fluxes. After optimisation of the CH_4 fluxes, the PFT parameters were manually adjusted to bring the PFT BF (PFT biomass as a fraction of total biomass) in line with observed aerial cover fraction ratios. These adjusted parameters are described as being an adapted parameter in Table S2. The calibrated model parameters and the necessary input files used to simulate the two peatland sites evaluated in this study are accessible from the bitbucket repository, bitbucket.org/tlippmann/pvn_public.

https://doi.org/10.5194/gmd-2023-48
Preprint. Discussion started: 29 March 2023

Geoscientific Model Development Discussions
Open Access
EGU

Table 3. A summary of the varied input data used to understand the sensitivity of the model. *To compare the PFT dynamics, both simulations use the 'no harvest' regime. The exchange of PFTs means that the model simulation driven by the Ilperveld input data (Table 4) will use the PFTs observed at the Horstermeer site (*Typha*, tall grass, sedges, brown moss PFTs) while the model simulation driven by the Horstermeer input data (Table 4) will use the PFTs observed at the Ilperveld site (short grass, tall grass, *Sphagnum*, brown moss PFTs).

Changing input variable	Input change
Air temperature	± 1 °C, ± 3 °C
Harvest frequency	no harvest; once, twice, three, and four times per year
PFTs	Exchange Ilperveld and Horstermeer PFTs*
Radiation	± 8 J m^{-2}, +100 J m^{-2}, +200 J m^{-2}
Water level	± 0.1m, ± 0.2m

2.5 Testing the PVN model

To understand the sensitivity of net CO_2 and CH_4 fluxes to PFT dependent processes, we conducted several model simulations using modified input data. We tested the sensitivity of PFTs processes to air temperature, water level, radiation, and harvest schemes by varying these inputs one by one (summmarised in Table 3).

To understand how the new model mechanisms affect emissions, we performed additional simulations with altered model algorithms and compared these to the original model simulations calibrated for the Horstermeer and Ilperveld sites. For example, the contribution of competition for shading to the overall simulation result, is quantified by comparing an altered simulation where incoming photactive radiation (PAR) is independent of shading (e.g. fractional par or FPAR = 0.25 for a simulation with four PFTs) to the original model simulations. We calculated the relative difference of the simulation with shading minus the simulation without shading. Similarly, we compared simulations with and without plant transported CH_4, with and without dynamic BF, with and without variable height.

In order to demonstrate that the PVN model reproduces CH_4 and CO_2 fluxes within the spread of observed fluxes when driven by realistic input data, we compared the modeled and measured CH_4 and CO_2 fluxes for two sites, the Horstermeer and the Ilperveld field sites, in North Holland, the Netherlands (Sect. 2.4).

We compare the CH_4 and CO_2 fluxes simulated by the new PVN model against the CH_4 and CO_2 fluxes simulated by the Peatland-VU model to understand the impact of introducing PFTs on the simulation of CH_4 and CO_2 fluxes. These model simulations are summarised in Table 4. Attempts to run the Peatland-VU model with new calibrated parameters did not yield results in the same order of magnitude as the observations. Therefore, it was necessary to use different model parameterisations for the PVN and Peatland-VU models.

2.6 Flux measurements

Carbon dioxide and CH_4 fluxes were measured using 2-4 automated flux chambers (AC) and the Los Gatos Gas Analyser, aligned with standardised chamber technique measurement protocol (Pavelka et al., 2018). Chambers were 30cm wide and 40cm in height, made of transparent acrylate, equipped with a fan and installed in the field using collars. Where necessary, vegetation was folded gently to fit inside the measurement chambers. Collars were removed from the field between sampling

https://doi.org/10.5194/gmd-2023-48
Preprint. Discussion started: 29 March 2023

Geoscientific Model Development Discussions

Table 4. A summary of the model simulations, using both the new PVN model and the pre-existing Peatland-VU (PV) model. PVN is an alphabetisation for the Peatland-VU-NUCOM v1.0 model. PV is alphabetisation for the Peatland-VU model.

Site	Model	Vegetation	Harvest height	Soil Profile	WL Input
Horstermeer	PVN	*Typha*, sedges, tall grass, brown moss	-	Horstermeer	Horstermeer
Horstermeer	PV	-	-	Horstermeer	Horstermeer
Ilperveld	PVN	Short grass, tall grass, brown moss, *Sphagnum*	0.15m	Ilperveld	Ilperveld
Ilperveld	PV	-	0.15m	Ilperveld	Ilperveld

campaigns which minimises disturbance which can lead to potential biases in the observations. This also potentially introduces uncertainty as to the precise measurement location. Measurements were recorded 24 $\mathrm{hr day}^{-1}$ for a week at a time, upon which the AC system was moved to another site. We note that due to the labor intensive nature of accumulating chamber observations consistently through time, these observational datasets do not offer complete temporal continuity, creating an intermittency bias. The CO_2 and CH_4 concentrations were measured inside the chamber, whilst the chamber was closed, during 15 minute intervals. From this data, the daily hourly average CO_2 (net ecosystem exchange) and CH_4 fluxes were calculated. To evaluate the model, we compared simulated and observed daily hourly average CO_2 and CH_4 fluxes. To estimate the degree of uncertainty, daily standard deviations were derived from the hourly fluxes. The values for all GHG emissions are expressed as CO_2 equivalents ($\mathrm{kgCO_{2eq} m^{-2} yr^{-1}}$) and calculated as

$$GHG_{CO_2e} = CH_4 \cdot GWP + CO_2 \tag{28}$$

where,

GWP_{20} = 80.8, as 1 $\mathrm{kgCH_4}$ = 80.8kg CO_2eq, over a 20 year time horizon, and

GWP_{100} = 27.2, as 1 $\mathrm{kgCH_4}$ = 27.2 kg CO_2eq, over a 100 year time horizon (Masson-Delmotte et al., 2021).

2.7 Input data preparation

Daily temperature and radiation data, measured at Schiphol, the nearest KNMI weather station was used as climate input data for both sites (accessed via https://www.knmi.nl/nederland-nu/klimatologie/daggegevens, last accessed 18 May 2022) (Fig. S2). The annual average rainfall at Schiphol, was 850 mm yr^{-1} over the period, 1990-2020, with 30% of the rainfall falling in summer and autumn, respectively, and 24% falling in winter, with the remainder falling in the spring. The average daily temperature between 1990 and 2019 was 9.4 °C and warmed approximately +0.1 $^{\circ}\mathrm{C yr}^{-1}$ over the same period. The average daily temperature for the warmest month, August, was 22.1 °C and the lowest daily monthly temperature for the coldest month, January, was 0.8 °C. Soil profile data from the Horstermeer and Ilperveld field sites was collected in 2015 and 2016 and includes DBD, C content, SOM content, sand and clay content, pF curve. Water level input data was sourced from the Dutch hydrological model, Netherlands Hydrological Instrument (NHI) (De Lange et al., 2014). The NHI water level output was converted to relative surface height using the digital elevation map, Actueel Hoogtebestand Nederland (Alhoz et al., 2020). The required input data for both peatland sites is accessible from the bitbucket repository, bitbucket.org/tlippmann/pvn_public.

https://doi.org/10.5194/gmd-2023-48
Preprint. Discussion started: 29 March 2023


Geoscientific Model Development Discussions

3 Results

The sign convention in this paper is that a positive gas flux is indicative of the flux entering the atmosphere and a negative flux is indicative that the flux is from the atmosphere. When describing on the annual CO_2, CH_4, and GHG values, we opt to use the term emissions, e.g. 'the total annual GHG emissions', whereas, when describing daily values, we opt to refer to these as fluxes, e.g. 'the daily GHG fluxes'. The goal of this study is not to create a new peatland emissions model to outperform the Peatland-VU model but to develop a new model capable of understanding the role dynamic PFTs have on CO_2 and CH_4 emissions in peatlands and for this reason, we do not aim to produce a new model to outperform the Peatland-VU model but a model that uses new dynamic processes where the model skill may be comparable to that of the Peatland-VU model.

3.1 Model sensitivity to input data

To understand the response of the modeled PFT processes to input data, we ran simulations with modified water levels (Fig. 3 and Fig. S5), temperature (Fig. 2 and Fig. S4), radiation (Fig. S6) input and harvest schemes (Fig. 4). The modified input data is summarised in Table 3 and the results of these sensitivity tests are summarised in Table 5. These results are indicative of the model mechanistic responses rather than projections on how PFTs might respond under varied environmental conditions. To show how different inputs impact plant processes, we present the belowground CO_2 emissions (Fig. 3), plant transported CH_4 (Fig. 2), above-ground biomass (Fig. 4). In the PVN model, the abundance of each PFT varies through time depending on the favourability of growing conditions. Therefore, an increase in CO_2 or CH_4 fluxes may be due to increased abundance (i.e. enhanced biomass) or enhanced transport efficiency. To disentangle this difference, the CO_2 and CH_4 fluxes for each PFT are plotted as a fraction of litter and root mass.

Warming air temperatures had a positive effect on both plant transported CH_4 emissions and litter & root mass at both sites Fig. S4. Short and tall grasses showed similar responses to warming air temperatures by producing large CH_4 emissions per kg of litter and root mass. Brown mosses showed little variation between the temperature experiments for the Ilperveld site but showed a decrease in fluxes with warming temperatures per kg of litter and root mass at the Horstermeer site. *Sphagnum* similarly showed a decrease in CH_4 fluxes with warming temperatures per kg of litter and root mass at the Ilperveld site. This decrease is because moss PFTs have strict ideal temperature growth limits and were limited by warming temperatures. Whilst belowground CH_4 concentrations increased with warming temperatures, the biomass, litter, and root mass of moss PFTs did not increase with warming temperatures.

Below-ground CO_2 emissions were impacted by changing water levels (Fig. S5). Previous studies have found that below-ground CO_2 production tends to increase with low water levels due to enhanced potential for aerobic CO_2 production (Knox et al., 2015). The results of the Ilperveld site sensitivity simulations showed that belowground CO_2 production increased with low water levels, likely due to enhanced potential for aerobic CO_2 production. However, the results of the Horstermeer site sensitivity simulations showed the converse, that the net CO_2 (5) and belowground CO_2 production increased with high water levels. We simulate that with high water levels, the reduced aerobic CO_2 production can be exceeded by the enhanced oxidation of CH_4 into CO_2. The large amounts of CH_4 oxidised into CO_2 in the Horstermeer site simulation are due to the very

https://doi.org/10.5194/gmd-2023-48
Preprint. Discussion started: 29 March 2023

Geoscientific Model Development Discussions
Open Access
EGU

Table 5. The results of the sensitivity testing. The CH_4 and CO_2 columns indicate how much the respective emissions changed when the input changed, relative to the results of the respective default Horstermeer and Ilperveld PVN simulations described in Table 4. A dash [-] indicates the simulation is the default site simulation. An overview of the sensitivity tests can be found in 3.

Changing input variable	Input change	Horstermeer		Ilperveld	
		CH_4 [%]	CO_2 [%]	CH_4 [%]	CO_2 [%]
Air temperature	+3°C	165	117	115	122
	+1°C	128	94	102	108
	-1°C	77	93	100	87
	-3°C	56	66	154	53
Harvest frequency	no harvest	-	-	120	129
	1 $year^{-1}$	114	68	87	117
	2 $year^{-1}$	114	67	-	-
	3 $year^{-1}$	115	67	152	70
	4 $year^{-1}$	114	68	185	45
PFTs	*Typha*, sedges, tall grass, brown moss	-	-	291	294
	Short grass, tall grass, brown moss, *Sphagnum*	35	68	-	-
Radiation	+200 J m^{-2}	121	107	97	126
	+100 J m^{-2}	111	104	98	113
	+8 J m^{-2}	101	101	98	101
	-8 J m^{-2}	99	99	98	99
Water level	+0.2m	149	104	200	99
	+0.1m	134	103	172	100
	-0.1m	98	98	87	101
	-0.2m	163	97	281	101

degraded peat present at the site (represented by low soil OM content in the soil input file) and the strong upwelling of rich groundwater at the Horstermeer site (represented by a site specific parameter which influences the sensitivity of aerobic CO_2 production). The large observed CH_4 emissions at the Horstermeer site are partially due to high CH_4 concentrations in the upwelling water. Furthermore, the large root systems of plants such as *Typha*, sedges and tall grasses have greater potential to access and transport stores of below-ground gases (represented by the PFT root depth and density). The conflicting response of the tall grass PFT in the Ilperveld and Horstermeer simulations shows that PFTs may respond differently to changing water levels at different sites.

Increasing the frequency of harvests led to a strong negative effect on vascular plant biomass and a small positive effect on moss plant biomass (Fig. 4). Biomass of non-moss PFTs is strongly impacted by the occurrence of harvests as indicated by the pause in biomass accumulation after harvest. However, by reducing tall vegetation, moss species have greater access

https://doi.org/10.5194/gmd-2023-48
Preprint. Discussion started: 29 March 2023

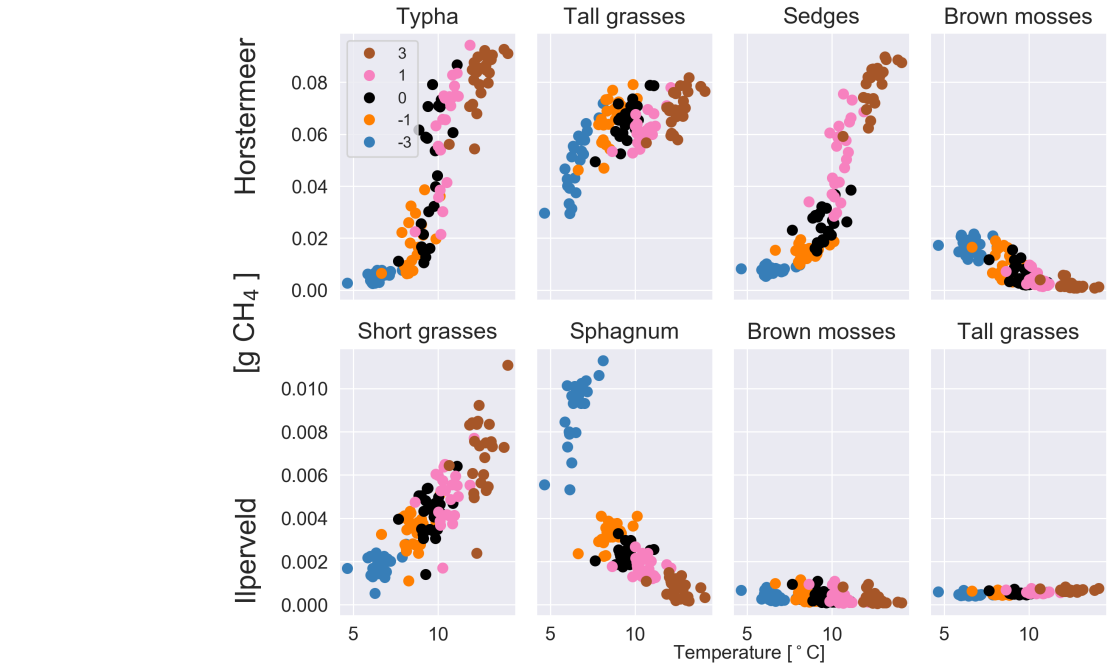

Figure 2. The results of the sensitivity tests show the relationship between different temperature inputs and the mean annual daily plant transported CH_4 (shown as a fraction of the mean annual daily litter & root mass), for each of the PFTs at the Horstermeer site (top row) and Ilperveld site (bottom row). Temperature input was increased and decreased by 1 & 3 °C, respectively. The legend shows the input change in °C where, ± signs in front of the legend labels show the direction of change. Note the different y axes between the top and bottom panels.

to sunlight and therefore, gain an advantage. For this reason, we saw the biomass of moss PFTs increase with more frequent harvests. In the Horstermeer site simulation, the greatest effect on biomass was between no harvests and the once per year harvests. In the Ilperveld site simulation, the effects of harvests on biomass increased somewhat linearly, according to the frequency of harvest events. We suspect that this is due to the inclusion of different PFTs in the two site simulations. In the Horstermeer site simulation, three PFTs have the capacity to grow above the harvest height (the *Typha*, tall grass, and sedge PFTs) whereas in the Ilperveld site simulation only tall and short grasses have the potential to grow beyond the harvest height, thereby limiting the potential effect harvests can have on the PFTs present. Furthermore, the growth of the short grasses PFT is height limited to 0.3m. Overall, total biomass was reduced with more frequent harvest regimes. It's important to note that whilst CO_2 emissions reduced by increasing the frequency of harvests (5), these emissions are not accounting for the off-site decomposition of harvested biomass.

3.2 Assessment of model mechanisms

To understand the role of isolated model mechanisms, we modified the model code to disable the functions responsible for reproducing the vegetation dynamics within in the model (Fig. 5). Unlike the simulations assessed throughout this paper, the simulation results shown in Fig. 5 begin in the year 1990. i.e. without the use of a spin up period. Removing the spin up period

https://doi.org/10.5194/gmd-2023-48
Preprint. Discussion started: 29 March 2023

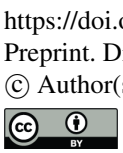

Geoscientific Model Development Discussions
Open Access
EGU

Figure 3. The results of the sensitivity tests show the relationship between different water level inputs and the mean annual daily below-ground CO_2 flux (shown as a fraction of the mean annual daily litter & root mass), for each of the PFTs at the Horstermeer site (top row) and Ilperveld site (bottom row). Water level input was decreased by 0.1 & 0.2 m and increased by 0.1 & 0.2 m, respectively. The legend shows the input change, where $\pm$ signs in front of the legend labels indicate the direction of change. Note the different y axes between the top and bottom panels.

showed that the modified model simulation results produce similar emissions in the first year of the simulation (1990) and allows assessment of the trajectory of deviation.

Disabling the shading scheme (simulation PVN_HEIGHT_CONST) or biomass fraction scheme (simulation PVN_CF_CONST) led to only slightly enhanced CO_2 emissions, whereas disabling the FPAR scheme (simulation PVN_FPAR_CONST) led to large CO_2 emission differences. Surprisingly, the difference for the PVN_FPAR_CONST simulation is opposite in sign for the two site simulations, and larger for the Ilperveld simulation. This means that maintaining constant FPAR, led to a small enhancement of CO_2 fluxes in the Horstermeer simulation but a large reduction of CO_2 fluxes for the Ilperveld simulation. These results show that FPAR plays a large role on simulated CO_2 emissions. The results of Ilperveld PVN_FPAR_CONST simulation results also showed that the FPAR function has the potential to introduce large variability into the emission results. This is interesting to note because the PVN model showed limited skill reproducing the CO_2 emissions at the Ilperveld site. These results indicate that the function calculating FPAR plays a driving role on CO_2 emissions but particularly at the Ilperveld site. Further model developments may investigate ways to improve the representation of FPAR in the model. The PVN_FPAR_CONST simulations also led to enhanced CH_4 emissions for the Ilperveld simulation. It is likely that CH_4 production was enhanced due to increased stores of CO_2.

https://doi.org/10.5194/gmd-2023-48
Preprint. Discussion started: 29 March 2023

Geoscientific Model Development Discussions

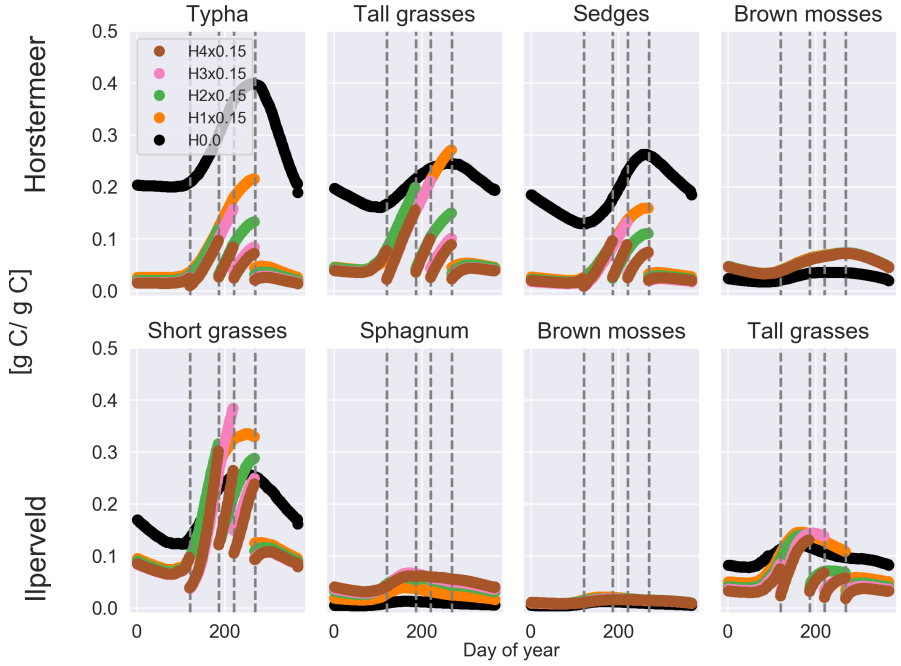

Figure 4. The results of the sensitivity tests show the relationship between different harvest schemes and biomass (shown as a fraction of the mean annual daily litter & root mass) for each day of year at the Horstermeer site (top row) and Ilperveld site (bottom row). Vegetation was cut to 0.15m at the moment of harvest. The legend shows the harvest input scheme. The dotted vertical lines indicate the four possible harvest days; day 120, 186, 220 and 268. Harvest was set to either not occur (H0.0), occur once per year (H1x0.15) on day 268, twice per year (H2x0.15) on days 186 and 268, three times per year (H3x0.15) on days 120, 220 and 268, or four times per year (H4x0.15) on all harvest days.

The use of the Peatland-VU CH_4 scheme (PVN_CH4_OLD_CF) led to large differences in CH_4 emissions for both the Horstermeer and Ilperveld simulations, in comparison to the PVN model results. The CH_4 emissions of the model simulations that use the Peatland-VU CH_4 scheme (simulation PVN_CH4_OLD_CF) were small when compared to the CH_4 emissions of the PVN model, for both model simulations. This indicates that the (PFT) modifications to the CH_4 scheme have led to substantial impacts on modeled CH_4 emissions.

3.3 Assessment of calibrated model simulations

Here, we describe the simulation results of the model calibrated at two field sites, the Horstermeer and Ilperveld. We describe the net annual CH_4 and CO_2 emissions, and GHG budgets (Fig. 6), as well as simulated PFT dynamics as indicated by changes to LAI, above-ground biomass, litter mass, and PFT height/depth (Fig. 7 and Fig. S7). All net GHG values are expressed as CO_2 equivalents (CO_{2eq}) and calculated using 20 (100) year GWPs using equation (28). The model simulation results indicate that the simulated annual mean net GHG emissions from the Ilperveld simulation were approximately half the emissions of the Horstermeer simulation. However, these model emission estimates are not considering off-site decomposition

https://doi.org/10.5194/gmd-2023-48
Preprint. Discussion started: 29 March 2023

Geoscientific Model Development Discussions
Open Access
EGU

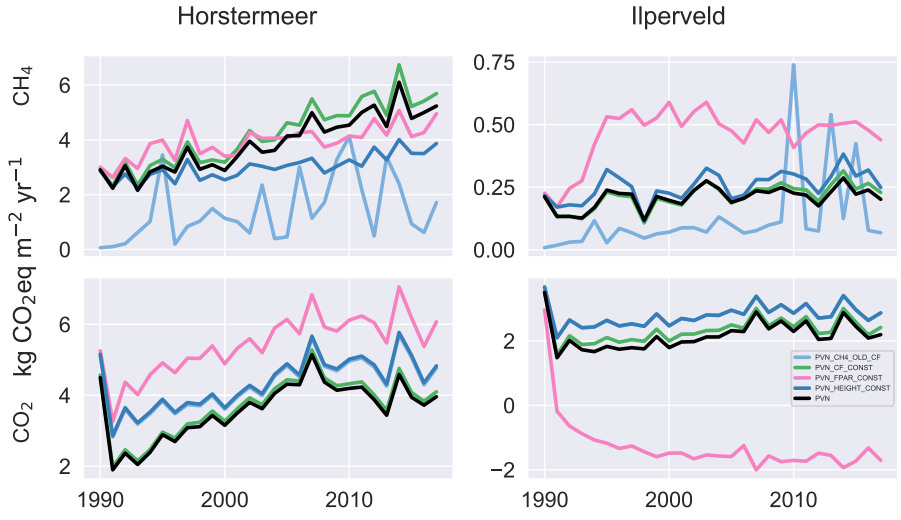

Figure 5. The CH_4 and CO_2 emissions for various isolated model mechanisms, compared against the PVN model result. We investigated maintaining constant fractional PAR (PVN_FPAR_CONST), maintaining constant plant height (PVN_HEIGHT_CONST), maintaining constant cover fraction (PVN_CF_CONST), and including the original Peatland-VU CH4 module multiplied by the PFT cover fraction (PVN_CH4_OLD_CF), at each time step.

of harvested biomass. The model estimated that the 1995-2017 annual average net GHG emissions were 2.4 (2.3) and 8.0 (5.2) $\mathrm{kgCO_{2eq}m^{-2}yr^{-1}}$ for the Ilperveld and Horstermeer model simulation results, respectively (Fig. 6). The model estimated that the 2015-2017 annual average net GHG emissions were 2.5 (2.3) and 8.9 (5.6) $\mathrm{kgCO_{2eq}m^{-2}yr^{-1}}$ for the Ilperveld and Horstermeer simulations, respectively (Table 6).

Assessment of the Horstermeer simulation showed that on average, CH_4 contributed approximately half (52%) of the net annual GHG emissions of the Horstermeer simulation, where CH_4 contributed 4.2 $\mathrm{kgCO_{2eq}m^{-2}yr^{-1}}$ and CO_2 emissions contributed 3.8 $\mathrm{kgCO_{2eq}m^{-2}yr^{-1}}$, on average. Assessment of the Ilperveld simulation showed that CO_2 was the primary contributor to net GHG emissions, where CO_2 contributed the majority (92%) of the annual GHG emissions (2.2 $\mathrm{kgCO_{2eq}m^{-2}yr^{-1}}$ of the total 2.4 $\mathrm{kgCO_{2eq}m^{-2}yr^{-1}}$ net GHG emissions). These model emission estimates neglect the off-site decomposition of harvested biomass. Therefore, CO_2 and CH_4 emissions are equally contributing to the net GHG emissions in the Horstermeer simulation, whereas, CO_2 emissions dominate the GHG emissions in the Ilperveld simulation results.

To assess whether there was an increasing or decreasing trend in emissions over the duration of the simulation (1995-2017), we calculated the linear regression of the CO_2, CH_4, and net GHG time series of the simulation results at both sites. The trend of Horstermeer simulation emission results was 0.13, 0.06, and 0.19 $\mathrm{kgCO_{2eq}m^{-2}yr^{-1}}$ for CH_4, CO_2, the net GHG emissions. Daily temperature observations show local temperatures increased by +0.1C $^{\circ}\mathrm{Cyr^{-1}}$ between 2010 and 2017, or +0.06 $^{\circ}\mathrm{Cyr^{-1}}$ over the entire simulation period (1995-2017). The trend results for the Ilperveld simulation emissions were zero for CH_4 emissions, and 0.04 $\mathrm{kgCO_{2eq}m^{-2}yr^{-1}}$ for CO_2 and net GHG emissions. Warming temperatures are a possible driver of the enhanced GHG emissions at the Horstermeer site. The increase in GHG emissions of the Horstermeer site simulation and the little or no increase of the Ilperveld site simulation are aligned with the results of the +1°C temperature sensitivity

https://doi.org/10.5194/gmd-2023-48
Preprint. Discussion started: 29 March 2023

Geoscientific Model Development Discussions
Open Access
EGU

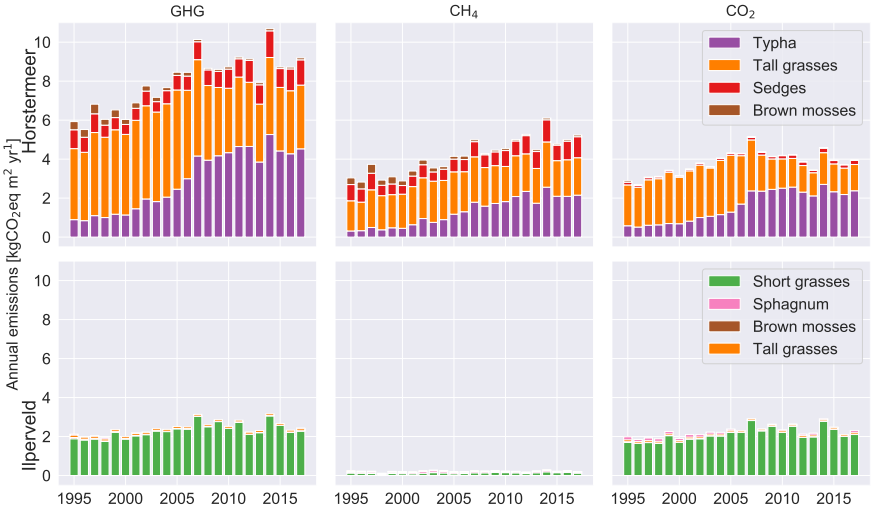

Figure 6. Relative contributions of each PFT to simulated annual average net GHG (left), CH_4 (middle), and CO_2 (right) emissions. The results of the Horstermeer site simulation are represented in the top row and the results of the Ilperveld site simulation are represented in the bottom row.

tests. The results of the Horstermeer site sensitivity tests showed that the *Typha* and sedge PFTs were sensitive to warming temperatures, and therefore the increase in the biomass and GHG emissions of the *Typha* and sedge PFTs at the Horstermeer site are likely due to enhanced temperatures.

3.3.1 PFT dynamics

Here we describe the living biomass, LAI, litter layer, biomass fraction, and height changes of the PFTs of the calibrated Horstermeer and Ilperveld model simulations (Fig. 7 and Fig. S7). Assessment of above-ground biomass (top row of Fig. 7) shows that the tall grass (blue line), *Typha*, and sedge PFTs (red line), were abundant during the Horstermeer simulation whereas the Ilperveld simulation was dominated by the short grass (green line), *Sphagnum* (pink line) and tall grass PFT (blue line). All plants showed seasonal variability. The ratio of the litter layer to biomass, is between approximately 1:4 and 1:3 for most PFTs (kgC). The *Typha* PFT is an exception, and the ratio is approximately 1:1. Overall, the sedge PFT showed comparable seasonal variability to the tall grass PFT whilst maintaining less biomass, smaller LAI, and shorter height throughout the Horstermeer simulation. The similar behaviour of the *Typha*, sedge, and tall grass PFTs were expected because the PFT input parameters represent similar plant phenologies. Assessment of the size of the litter layer (first row of Fig. S7) showed that in the Ilperveld simulation, the PFTs reached peak litter during Autumn (September) whilst in the Horstermeer simulation which is not mown, the litter continued to accumulate until January where rates of decomposition exceeded accumulation. The LAI (second row of Fig. S7) displayed strong seasonal variability. Each year, the LAI of the Short grasses reaches its maximum LAI value of 1.2. The tall grass PFT, whilst very competitive in the Horstermeer simulation is less competitive in the Ilperveld simulation, partially due to the occurrence of harvests and partially because it is out-competed by the fast growing short grass

https://doi.org/10.5194/gmd-2023-48
Preprint. Discussion started: 29 March 2023

Geoscientific Model Development Discussions
Open Access
EGU

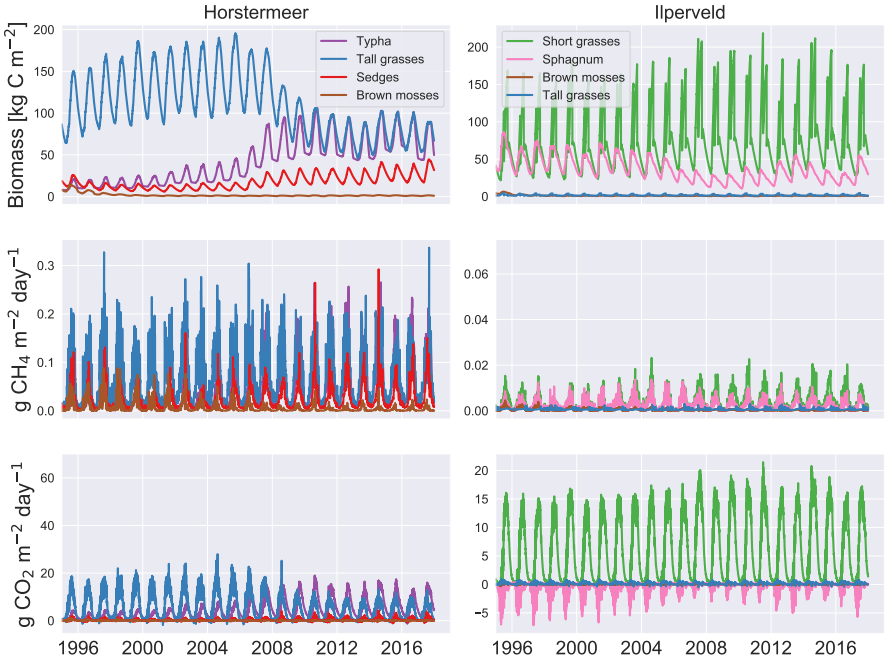

Figure 7. Vegetation dynamics. The results of the Horstermeer site simulation are represented in the left column and the results of the Ilperveld site simulation are represented in the right column. Note the differing y axes.

PFT. Assessment of the Ilperveld simulation reveals that the short grass PFTs were limited by maximum height. The tall grass PFT was not limited by the maximum height PFT parameter in the Ilperveld simulation but was instead limited by the biannual mowing regime. PFT height showed strong seasonal variability for both simulations (third row of Fig. S7). The tall grass PFT was the tallest plants in the Horstermeer simulation until 2009 and its height was frequently limited by the PFT maximum height input parameter. However, as the *Typha* PFT grew in biomass, the tall grass PFT appeared to have less access to sunlight as height and biomass values reduced. The *Typha* and sedge PFTs were not limited by their maximum height parameters. These changes in biomass fraction are also evident in the emissions.

The relative contributions of each PFT towards the and net annual CH_4, CO_2, and GHG emissions are shown using histogram plots (Fig. 6) where the CH_4 emissions refer to only the plant transported CH_4. The net CO_2 emissions for each PFT are the sum of the photosynthesis minus respiration, the CO_2 produced by belowground aerobic decomposition of inert SOM, and a portion of CH_4 oxidised to CO_2. The tall grass (red boxes), sedge (orange boxes), and *Typha* (purple boxes) PFTs are large transporters of CH_4 emissions of the Horstermeer simulations results. However, only the tall grasses and *Typha* compose the net CO_2 emissions in the Horstermeer simulation. Thereby, the tall grass PFT was the largest contributor to the net annual GHG emissions, followed by the *Typha* and sedges PFTs. The Ilperveld simulation results showed that the short grass PFT was the largest contributer to the net annual CH_4, CO_2, and GHG emissions.

https://doi.org/10.5194/gmd-2023-48
Preprint. Discussion started: 29 March 2023

Geoscientific Model Development Discussions
Open Access
EGU

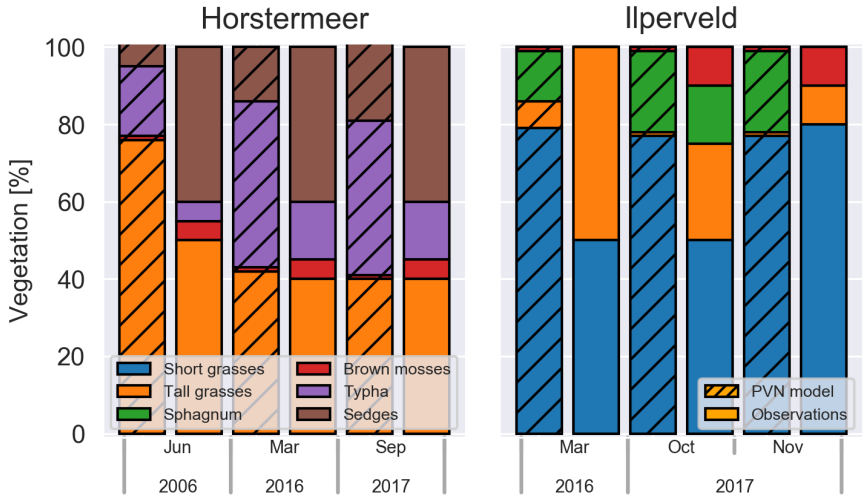

Figure 8. Simulated PFT biomass fractions and observed areal cover fractions at Horstermeer (left) and Ilperveld (right).

3.4 Comparison of modelled and observed plant dynamics

We compare simulated PFT biomass fractions against observed aerial plant cover fractions (Fig. 8). For assessment against observational data we compare model simulation results against observed fluxes by comparing time series, box plots, and 1:1 scatter plots for CH_4 (Fig. 9) and CO_2 (Fig. 10). Gaps in observational data exist due to measurement collection limitations, and therefore the model comparison against observational data can only be shown for the days where observational data exist. Unfortunately, this means that the model was not assessed equally across all seasons or, on the same days of the year at the two sites. For these reasons, the 1:1 plots, and R^2 linear regression results may only give a flavor of model performance. To understand the degree of uncertainty of the observational measurements, daily standard deviations were derived using the hourly fluxes (plotted as black error bars in Fig. 9 and Fig. 10). In each case the model simulation results generally lay within the spread of observational uncertainty. The observations indicated that both sites are annual sources of CH_4 and CO_2, and therefore, net annual sources of carbon to the atmosphere. The Horstermeer site (purple line in Fig. 9) and CO_2 (Fig. 10) produced large annual mean CH_4 and CO_2 emissions in comparison to the Ilperveld site (green line in Fig. 9) and CO_2 (Fig. 10).

3.4.1 Evaluation of plant composition dynamics

Plant cover fraction observations were made at the location of the chamber measurements and were not representative of the site's plant complete community composition. Although aerial cover fraction and biomass fraction (the ratio of PFT biomass to total biomass) are not the same, changes in plant composition are depicted in both representations.

https://doi.org/10.5194/gmd-2023-48
Preprint. Discussion started: 29 March 2023


Geoscientific Model Development Discussions

In 2006, the chamber measurement location at the Hostermeer field site was composed of tall grasses (50%), sedges (40%), *Typha* (5%), and brown mosses (5%) (left panel in Fig. 8). The Horstermeer simulation results have good agreement with the observations but overestimated the amount of tall grasses (66%) and underestimated the amount of Sedges (40%). In 2016, a decade later, the amount of tall grasses remained consistent, whilst the amount of *Typha* had increased by 10%. One year later in 2017, the vegetation had not undergone changes, proportionally. Parallel to the observations, the Horstermeer simulation results estimated that the tall grass PFTs decreased to 60%, from 2005 onwards whilst, the biomass fractions of the *Typha* and sedge PFTs increased. Overall, the Horstermeer simulation overestimated the biomass fraction of the tall grass PFT, and underestimated the proportion of the sedges and *Typha* PFTs. Model estimates of year-to-year PFT biomass changes were of the same sign and similar magnitude as in situ observations.

In March 2016, the chamber measurement location at the Ilperveld field site hosted short grasses (50%) and tall grasses (50%). The model overestimated the amount of short grasses (80%), underestimated the amount of Tall grasses (5%), and overestimated the amount of *Sphagnum* (10%). The *Omhoog met het Veen* (Raising the Peat) project delivered onsite managements attempts to initiate *Sphagnum* growth by hand dispersing living fragments of *Sphagnum spp.* from a nearby donor site between 2013 and 2015 (Geurts and Fritz, 2018). For this reason, we expected that the model may not match the development of *Sphagnum* at the Ilperveld site. In October 2017, the vegetation shifted to be composed of short grasses (50%), and tall grasses (25%), *Sphagnum* (15%), and brown mosses (10%). One month later in November 2017, the *Sphagnum* was no longer visible (0%), brown mosses remained (10%), and the site was dominated by short grasses (80%). The model estimated that the short grass and *Sphagnum* PFTs remained consistent into 2016 and 2017, whilst the tall grass PFT reduced and brown mosses increased slightly. Whilst the model simulations ended in 2017, we saw that in October 2018, the vegetation remained constant at both sites.

3.4.2 Evaluation of simulated CH_4 fluxes

The time series' presented in Fig. 9 shows the behaviour of the Horstermeer simulation CH_4 flux results (purple line), the observed mean daily fluxes (black dots) and the spread of the hourly observed fluxes (black error bars). Whilst, the Horstermeer simulation reproduced the seasonal variability of the observed CH_4 fluxes, the box plots showed that the simulation results (purple box) tended to overestimate the CH_4 fluxes. Overall, the Horstermeer simulation showed a robust pattern of variability when compared with the observations (R^2 = 0.7) whilst overestimating the magnitude of observed fluxes. Assessment of the Ilperveld model simulation showed that the model was able to reproduce the observed CH_4 fluxes and followed the pattern of variability when compared with the observations (R^2 = 0.8). The summer of 2015 is an exception where the simulated results showed an increase in CH_4 fluxes, larger than the observed CH_4 fluxes. Assessment of the box plots showed that the simulated CH_4 fluxes (green box) are of similar mean and spread to the observed fluxes (purple box).

3.4.3 Evaluation of simulated CO_2 fluxes

The box plots showed that the PVN Horstermeer simulation reproduced the median and range of observed daily CO_2 fluxes at the Horstermeer site. The results of the Horstermeer site simulation (purple line) reproduced the 2015, 2016, 2017 Spring

https://doi.org/10.5194/gmd-2023-48
Preprint. Discussion started: 29 March 2023

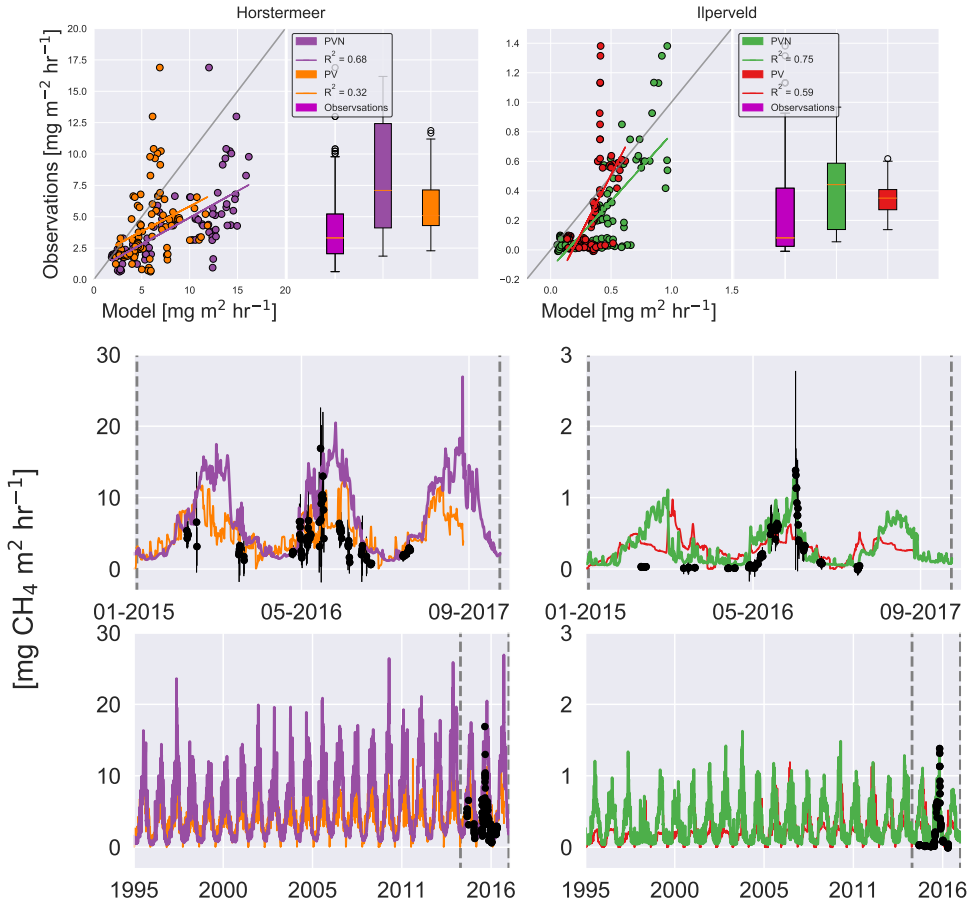

Figure 9. Simulated and observed methane fluxes at the Horstermeer (left) and Ilperveld (right). The R^2 values are provided for comparison between the new PVN, Peatland-VU model and the observations. In the top panel, the 1:1 line is plotted in grey. The black dots are in situ flux chamber observational measurements in the middle and lower panels. Note the differing x and y axes.

CO_2 fluxes. The results of the Horstermeer site simulation captured the 2015 and 2016 Autumn fluxes. However, the model generally overestimated the magnitude of simulated fluxes (purple box) but generally reproduced the variability (R^2 = 0.8).

The box plots in Fig. 10 showed that the Ilperveld simulation results (green box) generally overestimated CO_2 fluxes. The box plots showed that the daily mean hourly CO_2 flux simulated by the model was a small positive flux, 250mg $\mathrm{mgCO_2 m^{-2} hr^{-1}}$ whereas the observed mean flux was $0\,\mathrm{mgCO_2 m^{-2} hr^{-1}}$. The Ilperveld simulation (green line) captured the early Spring fluxes in 2016, and 2017. However, during 2015 and 2016, the model tended to overestimate the observed CO_2 fluxes. Comparison of the simulated daily hourly average (green line) and the spread of hourly fluxes (black error bars) showed that the simulated CO_2 fluxes (green line) fell within the spread of daily hourly fluxes. The model showed some agreement with the observed pattern of variability (R^2 = 0.6).

https://doi.org/10.5194/gmd-2023-48
Preprint. Discussion started: 29 March 2023

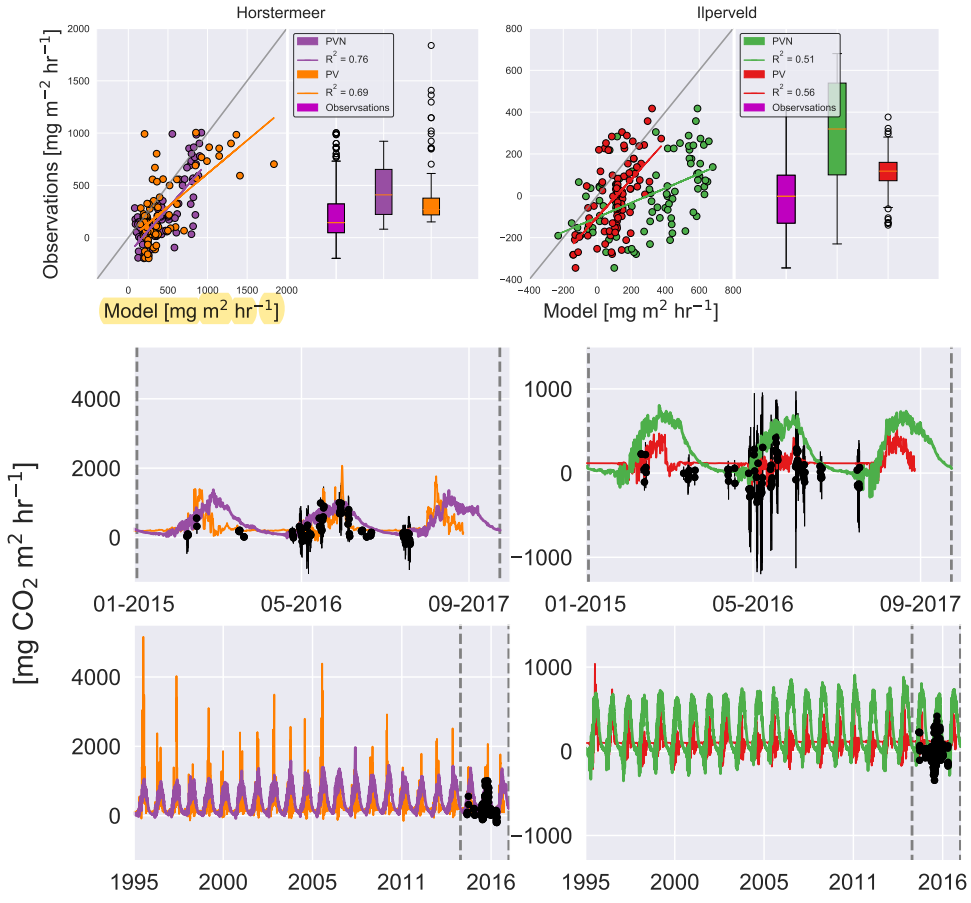

Figure 10. Simulated and observed carbon dioxide fluxes (NEE) at the Horstermeer (left) and Ilperveld (right). The R^2 values are provided for comparison between the new PVN, Peatland-VU model and the observations. In the top panel, the 1:1 line is plotted in grey. The black dots are in situ flux chamber observational measurements in the middle and lower panels. Note the differing x and y axes.

The comparison between the Horstermeer simulation results and observations showed that the model captured the mean daily CO_2 fluxes but overestimated CH_4 fluxes. The comparison between the Ilperveld simulation results and the observations showed that the model overestimated the mean CO_2 fluxes but reproduced the mean and variability of CH_4 fluxes.

3.5 Comparison to the PEATLAND-VU model

To understand the impact of including vegetation dynamics, we compare the results of the new PVN model against the results of the pre-existing Peatland-VU model (Fig. 9) and CO_2 (Fig. 10). The simulation results are summarised in Table 6. Overall, the PVN model estimated the net annual CH_4, CO_2, and GHG emissions to be larger than the emissions estimates made by the Peatland-VU model. The Peatland-VU model estimated the annual mean 2015-17 GHG emissions to be 1.3 and 5.9 $\mathrm{kgCO_{2eq}m^{-2}yr^{-1}}$ for the Ilperveld and Horstermeer simulations, respectively, calculated using a 20yr GWP. When

https://doi.org/10.5194/gmd-2023-48
Preprint. Discussion started: 29 March 2023

Geoscientific Model Development Discussions
Open Access
EGU

Table 6. Annual average 2015-17 and 1995-2017 CO_2, CH_4, and GHG emissions. All values are expressed as CO_2 equivalents ($kgCO_{2eq}m^{-2}yr^{-1}$) and calculated using 20 (100) year GWP for CH_4 and GHG values.

Site	Model	GHG		CO_2		CH_4	
		2015-17	1995-2017	2015-17	1995-17	2015-17	1995-17
Horstermeer	PVN	8.88 (5.56)	7.96 (5.20)	3.87	3.81	5.01 (1.68)	4.15 (1.40)
Horstermeer	PV	5.90 (3.80)	5.80 (3.81)	2.74	2.81	3.17 (1.07)	2.99 (1.01)
Ilperveld	PVN	2.47 (2.32)	2.41 (2.27)	2.25	2.19	0.22 (0.08)	0.22 (0.08)
Ilperveld	PV	1.27 (1.15)	1.19 (1.08)	1.09	1.03	0.18 (0.06)	0.16 (0.05)

calculated using a 100yr GWP, the Peatland-VU model GHG emission estimates for the Horstermeer simulation were 3.8 $kgCO_{2eq}m^{-2}yr^{-1}$ (for both periods 2015-17 and 1995-2017). The Peatland-VU GHG emission estimates for the Ilperveld simulation were 1.3 and 1.2 $kgCO_{2eq}m^{-2}yr^{-1}$, for the 2015-17 and 1995-2017 periods, respectively.

The comparison of modelled and measured CH_4 emissions showed that the PVN model performed well, reproducing CH_4 emissions within the spread of observations, in comparison to the Peatland-VU model. The PVN Horstermeer simulation results estimated large mean annual CH_4 emissions (5.1 $kgCO_{2eq}m^{-2}yr^{-1}$) in comparison to the Peatland-VU model (3.2 $kgCO_{2eq}m^{-2}yr^{-1}$) for the period 2015-17. The R^2 value of the PVN model results in comparison to the observations was 0.7 for the Horstermeer simulation and 0.8 for the Ilperveld simulation. In comparison, the Peatland-VU model results produced R^2 values of 0.3 and 0.6 for the Horstermeer and Ilperveld simulations, respectively. The Peatland-VU model showed good skill reproducing the CO_2 fluxes at the Horstermeer site (R^2 = 0.7) and less skill at the Ilperveld site (R^2 = 0.6). Similarly, the PVN model showed good skill reproducing daily CO_2 fluxes at the Horstermeer site (R^2 = 0.8) but less skill at the Ilperveld site (R^2 = 0.6), as indicated by the linear regression results. Overall, assessment of the linear regression results showed that the behaviour of the PVN model performed well against the observations when compared to the Peatland-VU model.

4 Discussion

We have developed the PVN model, a new dynamic vegetation-peatland-emissions model capable of understanding the role dynamic PFTs have on CO_2 and CH_4 emissions in peatlands. The aim of the PVN model is not to outperform the Peatland-VU model but to include representation of dynamic plant processes. For this reason, the model skill may remain comparable to that of the Peatland-VU model. We tested the sensitivity of simulated PFT processes to changing environmental parameters. We have assessed the impacts of the schemes introduced into the model that replicate competition between vegetation types. Here we discuss potential sources of uncertainty, both in the observational data used to evaluate the model results and in the chosen model input parameters. Secondly, we discuss the processes in the model that allow the representation of dynamic vegetation and the ability of these processes to respond to changing environments. Lastly, we discuus how the new PVN model compares to its two parent models, the NUCOM-BOG model and the Peatland-VU model, as well as the one other site-specific GHG emissions peatland model that uses dynamic PFTs.

https://doi.org/10.5194/gmd-2023-48
Preprint. Discussion started: 29 March 2023


Geoscientific Model Development Discussions

4.1 Sources of uncertainty

4.1.1 Input parameters

It is important to note that the Peatland-VU, NUCOM-BOG and PVN are heavily parameter dependent models. The Peatland-VU model has been shown to reproduce observed fluxes using widely different parameter sets which means that the Peatland-VU model has a strong equifinality of parametrisations (van Huissteden et al., 2009) because there is simply not enough data available to constrain all model dynamics. One aim of introducing PFTs into the Peatland-VU model was to develop a model with greater dependence on observational data (measured PFT traits) and less dependence on parameters. Thereby, the model performance against observed fluxes may be similar or only somewhat improved in comparison to what was achieved using the Peatland-VU model but the equifinality of the model may be less. It is important that improvements of model processes capture the critical processes, but as simply as possible to minimise problems that arise due to the equifinality of parametrisations (Beven and Freer, 2001).

4.1.2 Site Heterogeneity and chamber measurements

We compare the findings of this study against other studies that have assessed observed CH_4 fluxes at the Horstermeer site and discuss uncertainties accompanying the chamber measurement technique. Unfortunately, at the time of publication there were no published studies investigating the CO_2 or CH_4 fluxes measured at the Ilperveld site. The CH_4 fluxes observations (0-17 $\mathrm{mgCH_4m^{-2}hr^{-1}}$) presented in this study compared well to reported chamber CH_4 fluxes measured at the Horstermeer site from 2003 till 2008 (van Huissteden et al., 2009), in the range of 2-15 $\mathrm{mgCH_4m^{-2}hr^{-1}}$, at an area of the site with a varying water table. Interestingly, the CH_4 observations presented measured in a wet area of the Horstermeer site were more than double the measurements measured in dry areas of the Horstermeer between 2004 and 2006, using the manual chamber technique (Hendriks et al., 2007). The different chamber measurement locations used by the two studies may account for some of the observed differences. Heterogeneous vegetation and heterogeneous water levels relative to the surface are known to impact both automated and manual flux-chamber measurements. For this reason, observational measurements are impacted by the physical placement of flux chambers in the field, leading to potential measurement bias (Speckman et al., 2015; Baldocchi, 2003). At very heterogeneous sites, such as the Horstermeer site, flux strengths vary due to micro-topography (Wania et al., 2010) and chamber measurements have been reported to vary significantly within one site, which may explain differences between studies.

The Horstermeer site has vegetation standing taller than 1m. At times, it was necessary to consider the vegetation height when selecting chamber location to ensure vegetation (even when folded) could fit within measurement chambers. Field measurements that exclude areas covered by tall vegetation may result in a significant underestimation of CO_2 or particularly, CH_4 fluxes where, the absence of tall vegetation measurements limits the capacity to model tall vegetation processes and predict associated changes in CO_2 and CH_4 fluxes (Pangala et al., 2013), potentially influencing the CO_2 and CH_4 flux estimates. Due to the labor-intensive nature of accumulating chamber observations consistently through time, these observational datasets do not offer complete temporal continuity, creating an intermittency bias. The high cost of AC meant that sites could not be

https://doi.org/10.5194/gmd-2023-48
Preprint. Discussion started: 29 March 2023


Geoscientific Model Development Discussions

measured simultaneously, leading to an interrupted sampling regime that may bias CO_2 and CH_4 flux estimates (Morin et al., 2014a, 2017). Most chamber measurements were taken during the plant growing season, assuming that the winter fluxes are negligible which has been shown to not always be the case (Morin et al., 2014b). Future studies can benefit from continuous AC measurements.

4.1.3 On the efficacy of simulating dynamic vegetation

The PVN model was developed by building upon the functionality and structure of the Peatland-VU model whilst incorporating vegetation dynamics from the NUCOM model. The model has incorporated vegetation dynamics and enhanced the Peatland-VU model's existing carbon cycling processes. Competition is based on water table depth, temperature, vegetation height and shading. To verify that the model dynamics are robust and to understand the sensitivity of the PFTs, we performed model sensitivity simulations.

Considering that the short grass, *Sphagnum* and brown moss PFTs share similar PFT parameters, these three PFTs can respond somewhat similarly. Whilst, the short grass PFT is a non-moss PFT, its parameters are not dissimilar to those of moss PFTs. However, the short grass PFT quickly increases in biomass due to its broad temperature and water growth limits. This means that the short grass PFT provides strong competition against other PFTs. Even though the short grass PFT is height limited, its quickly increasing biomass allows increasing access to PAR, which leads to large amounts of plant respiration, root growth, and net CO_2 fluxes when compared to the *Sphagnum* and brown moss PFTs. With only a small root system (maximum 0.1m), moss PFTs have limited abilities to transport below-ground CO_2 and as expected, the total below-ground CO_2 flux is small for mosses. Key differences in the parameters between short grasses and brown mosses are that short grasses are not considered a moss (relevant for height growth and light interception), moss (short grass) PFTs have large (small) MethanePType value, whereas moss PFTs have low LeafRespirationCoeff and BiomassSenescence values. Whilst these differentiations have been somewhat effective, future model versions might consider further ways of distinguishing moss (especially *Sphagnum*) species. The presence of *Sphagnum* SOM increases the acidity of the soil. By influencing the acidity of the soil and limiting the nutrient availability, *Sphagnum* gains an advantage over other plant types because *Sphagnum* flourishes in nutrient poor conditions (Moore et al., 2007). A useful addition to future model versions may be to adapt the living moss layer to be incorporated into the soil layer, altering the height of the land surface (relative to the water table, for example) and corresponding soil properties (e.g. pH, DBD).

4.1.4 Impacts of changing temperature input

Studies show that whilst both CH_4 production and oxidation rates are enhanced by warming, the net CH_4 flux increases with warming because CH_4 production increases at a rate faster than oxidation (Granberg et al., 1999). As expected, the PVN model simulated enhanced (decreased) CH_4 emissions under simulations driven by warmer (cooler) temperatures. *Sphagnum*, tall grasses, and brown mosses showed unexpected results because they released less CH_4 emissions under warmer simulations. This may be indicative of the narrow temperature limits of *Sphagnum* moss. The impacts of temperature on model processes are three-fold. Firstly, the amount of photosynthesis, and plant respiration performed is dependent on the ideal and tolerated

https://doi.org/10.5194/gmd-2023-48
Preprint. Discussion started: 29 March 2023


Geoscientific Model Development Discussions

PFT growth temperatures. Secondly, the amount of litter converted to below-ground SOM reservoirs is dependent on soil temperatures, where warmer soil temperatures lead to larger amount of litter converted to below-ground reservoirs. Thirdly, decomposition of below-ground SOM is dependent on soil layer temperature (as well as pH, saturation etc.), where soil layers closer to the surface are warmer. Thereby, temperature influences the PFT abundance, size of litter and below-ground SOM reservoirs available for decomposition, and the efficiency of below-ground SOM decomposition in the model. Field studies which have shown relationships between individual species, CH_4 emissions, and carbon turnover (*Carex*, *Phragmitis*, and *Typha* (Günther et al., 2015); *Eriophorum vaginatum*, *Carex rostrata* and *Juncus effusus* (Ström et al., 2005)).

4.1.5 Belowground decomposition

Enabling different PFTs to contribute to, oxidise, and decompose different below-ground SOM pools, impacted simulated CO_2 and CH_4 fluxes. Decomposition in the PVN model is dependent on the decomposition rates of different PFTs. Decomposition rates generally follow this order: forbs, graminoids, deciduous shrubs, evergreen shrubs (Dorrepaal et al., 2006, 2007, 2009). The peat-SOM pool of moss PFTs contribute to CO_2 and CH_4 fluxes because (*Sphagnum*) mosses are the primary peat-contributing plant and mosses (especially *Sphagnum*) have slow decomposition rates (Hobbie et al., 2000). Moss PFTs are the only PFTs able to contribute to the peat SOM pool which means that the CH_4 fluxes arising from decomposition of the peat SOM pool are only transferred to the surface by moss PFTs. Future modelling efforts could work to improve the representation of peat decomposition, whereby CO_2 fluxes resulting from the decomposition of peat can be transferred to the surface by both moss and non-moss PFTs. Mosses are prescribed to have maximum 0.1m roots when the model is initialised and remain constant throughout the model simulation. Mosses do not have an above-ground litter layer and instead their living biomass after senescence, is added directly to the below-ground SOM.

4.1.6 Impacts of changing water level input

Largely, decomposition of the peat reservoir led to enhanced CO_2 fluxes, due to a large aerobic layer, with low water levels. Plant transported CH_4 and aerobic CO_2 production process are dependent on root mass and independent on above-ground biomass. In the model, the below-ground CO_2 flux is comprised of CO_2 produced by peat, root exudates, litter, roots, microbial biomass, humic matter, and CH_4 oxidation. Root traits play an important role in species competition (Iversen et al., 2015) and use of observational data, such as exudation rates, root mass and shoot mass, would help constrain future versions of the model. Modeled photosynthesis and leaf respiration are independent of water levels because the photosynthesis production model is temperature and not water dependent. Whilst, this may produce representative results in systems that are not water-limited, future model versions may consider the relationship between water availability and plant growth, and particularly the impacts of drought on both plant photosynthetic capacity and respiration.

https://doi.org/10.5194/gmd-2023-48
Preprint. Discussion started: 29 March 2023


Geoscientific Model Development Discussions

4.1.7 The impact of harvests on plant competition

The inclusion of harvest has proven necessary to reproduce the seasonal variability of fluxes in grasslands and crops, where crop harvests occur (Van den Hoof et al., 2011). Whilst CO_2 emissions were reduced with increased harvest frequency, these emissions are not considering off-site decomposition of harvested biomass. The harvest method implemented in the PVN model was similar to the instantaneous harvest method featured in other dynamic vegetation models (such as JULES, Littleton et al. (2020)), where the plant is reduced to a certain set height and living biomass and LAI are subsequently adjusted accordingly. JULES assumes 100% of lost biomass is harvested whilst killing off a proportion of below- ground biomass that is converted to litter. The PVN model assumes 20% of harvested biomass is lost to litter and does not account for root death. The increased litter layer leads to enhanced emissions resulting from the decomposition of the litter layer. The PFT living biomass is reduced by the proportional biomass lost, assuming the plant's biomass is uniformly distributed with height, and LAI is recalculated. Root mass observational measurements over time as well as observational data on the impact of harvests on plant productivity would further improve model representations of harvests. Further assessment may investigate in what ways the photosynthesising, and gas conduit capacities of plants are further reduced in the days after harvest and how this can be better captured by the model.

4.2 Comparison to other site-specific peatland GHG emission models

Here we compare the functionality of the new PVN model against its parent models; the Peatland-VU and NUCOM-BOG models. We then also compare the functionality of the PVN model against functionality of PEATBOG, the one other site-specific peatland GHG emissions model that includes dynamic vegetation (Table S1).

We have developed a new model capable of understanding the role dynamic PFTs have on CO_2 and CH_4 emissions in peatlands and for this reason, we do not expect the PVN model to outperform the Peatland-VU model but that the model skill should, at least, be comparable to that of the Peatland-VU model. The PVN model simulation results estimated the 1995-2017 annually averaged net GHG budget to be larger than the Peatland-VU model, at both sites. We suspect that there are two reasons for this. The first being a trade-off between enhanced CO_2 fluxes or enhanced CH_4 fluxes. In both the Peatland-VU and PVN models, the CO_2 processes are calculated first. Calibration of the photosynthesis and plant respiration related parameters impacts the amount of CO_2 available for CH_4 production. We found that the CO_2 production scheme was the greatest cause of uncertainty in the model. Future model versions, may consider ways to constrain the net CO_2 flux by improving the response of photosynthesis to environmental variables. To improve upon this in future model versions it may be useful to consider the representation of below-ground carbon decomposition. The below-ground CH_4 pool in the Peatland-VU model increased consistently during the model simulation and therefore, an increasing quantity of CH_4 was released from the soil profile throughout the simulation, indicating that the fluxes were likely underestimated early in the simulation. The PVN model prescribes each PFT to have root and shoot mass and root depths. This enables each PFT to access different soil layers, and below-ground CH_4 and carbon pools, potentially impacting the longterm variability of CH_4 emissions. When compared to observed fluxes, the results indicated that the CO_2 scheme in the PVN model may have limited skill when applied to peatland sites of certain physical properties. These results cannot be compared with previous modelling studies because the Peatland-

https://doi.org/10.5194/gmd-2023-48
Preprint. Discussion started: 29 March 2023


Geoscientific Model Development Discussions

VU CO_2 production scheme results have not been published since the CO_2 production scheme was introduced by Mi et al. (2014) for assessment of the impact on simulated CH_4 fluxes.

The NUCOM model was developed to assess the impact of climate change on bog ecosystems by analysing simulations lasting 200-500 years. Running the model over time periods similar to the NUCOM's 1760–2000 simulation period, can assess the model's ability to reproduce shifts in vegetation in response to climate variability. This would require model evaluation using multi-centennial observational data, such as macrofossil evidence. To further investigate the impact of climate change on peatland ecosystems future studies may consider using macrofossil data in combination with forward or backward multi-decadal or multi-centennial climate projections.

The PEATBOG model (Wu and Blodau, 2013) is the one other site-specific peatland model that simulates CO_2 and CH_4 fluxes and includes competition between PFTs. The PEATBOG model simulated the Mer Bleue Bog in Canada, a pristine (untouched) raised acidic ombrotrophic bog, over a 6 year period. The Mer Bleue Bog is a nutrient poor bog, which is different to the two sites assessed in this study. Peat has been accumulating at this site since 8400 calyrBP and has developed a peat depth of 6m in the center. The PEATBOG model accounts for similar biogeochemical processes as the PVN model but beyond this also includes representation of the nitrogen cycling, and subsequent dissolved inorganic and organic carbon, CO_2 and CH_4 run-off. The PEATBOG model underestimated the annual net GHG emissions (net ecosystem carbon balance), by approximately half of observed field observations. The net annual GHG emissions for the Mer Bleue Bog site were small, approximately 0.02% of the GHG emissions observed at the Ilperveld field site in the Netherlands. Wu and Blodau (2013) noted the sensitivity of the PEATBOG model to temperature, reporting that $1^{\circ}C$ of temperature change was enough to initiate a model bias, swaying the model from a source to a sink. Plot-scale model inter-comparison efforts could help improve the representation of small-scale processes in peatland models. However, the breadth of observational data required to run and test site-specific models, make site specific model inter-comparison efforts cumbersome and difficult.

5 Conclusions

Peatlands are one of the most important carbon storing ecosystems. The challenges facing our understanding of the carbon balance and CH_4 dynamics subsequent to the rewetting of previously managed peatlands are numerous. One challenge is the ability of site-specific peatland models to reproduce methane fluxes, particularly in relation to plant functioning. This question is particularly timely because there exists an urgent need to restore drained peatlands to reduce land subsidence whilst limiting GHG emissions. Here, we present Peatland-VU-NUCOM v1.0 (PVN), a new site-specific peatland dynamic vegetation emissions model. PVN was designed to simulate plant competition above and below-ground, whilst developing carbon pools for the production and oxidation of CH_4 and CO_2. We showed that the PVN model was able to reproduce plant biomass fractions, CH_4 and CO_2 fluxes. This confirms that the model provides the capability to understand the relationship between peatland plant dynamics, CH_4 and CO_2 emissions. The PVN model is a relevant tool that can be used to optimize vegetation management with the goal to reduce GHG emissions.

https://doi.org/10.5194/gmd-2023-48
Preprint. Discussion started: 29 March 2023


Geoscientific Model Development Discussions

Code and data availability. PVN 1.0 source code is available at bitbucket.org/tlippmann/pvn_public (last access: 6 Mar 2023). All input data used to generate the model simulations presented in this study can be accessed through this Bitbucket. This includes site model parameterisations, site soil profiles, climate data, water level data, and PFTs. The exact version of the model source code used to produce the results presented in this paper is archived on Zenodo (https://zenodo.org/record/7701698, Lippmann and van Huissteden (2023)).

Author contributions. TL, KvH, and MH developed the theoretical framework of the model. TL performed the model developments, composed the PFTs, made the figures, all analyses, and wrote the paper. TL and KvH collected the observational data, developed the model parameterisation scheme, and soil profiles. KvH processed the observational data and offered valuable suggestions on the development and calibration of the model. YvdV offered valuable suggestions on testing of the model and presentation of analyses. HD participated in the writing of this paper. HD, MH, KvH,YvdV participated in the revision of this paper. DH, HD, MH, and KvH acquired the funding and administered this project.

Competing interests. The contact author has declared that neither they nor their co-authors have any competing interests.

Acknowledgements. We would like to thank the editor and the reviewers for their valuable comments and suggestions. We thank Merit van den Berg for proof-reading.

https://doi.org/10.5194/gmd-2023-48
Preprint. Discussion started: 29 March 2023

Geoscientific Model Development Discussions

References

Abdalla, M., Hastings, A., Truu, J., Espenberg, M., Mander, Ü., and Smith, P.: Emissions of methane from northern peatlands: a review of management impacts and implications for future management options, Ecology and Evolution, 6, 7080–7102, https://doi.org/10.1002/ece3.2469, 2016.

Alhoz, K., Kenesei, K., Papageorgiou, M., Keurentjes, E. E. M., and de Jong, M.: Improved AHN3 Gridded DTM/DSM, 2020.

Baldocchi, D. D.: Assessing the eddy covariance technique for evaluating carbon dioxide exchange rates of ecosystems: Past, present and future, Global Change Biology, 9, 479–492, https://doi.org/10.1046/j.1365-2486.2003.00629.x, 2003.

Beven, K. and Freer, J.: Equifinality, data assimilation, and uncertainty estimation in mechanistic modelling of complex environmental systems using the GLUE methodology, Journal of Hydrology, 249, 11–29, https://doi.org/10.1016/S0022-1694(01)00421-8, https://reader.elsevier.com/reader/sd/pii/S0022169401004218?token=84A0A21BA33A482EA3711C56C9EB53206FA532DC87BF9199C71F7CFD2C7FE71AF9077B53D9A3EA9AE8195593FCCAEA62&originRegion=eu-west-1&originCreation=20221223141626https://linkinghub.elsevier.com/retriev, 2001.

Boonman, J., Hefting, M. M., Van Huissteden, C. J., Van Den Berg, M., Van Huissteden, J., Erkens, G., Melman, R., and Van Der Velde, Y.: Cutting peatland CO2 emissions with water management practices, Biogeosciences, 19, 5707–5727, https://doi.org/10.5194/bg-19-5707-2022, https://doi.org/10.5194/bg-19-5707-2022, 2022.

Box, J. E., Colgan, W. T., Christensen, T. R., Schmidt, N. M., Lund, M., Parmentier, F. J. W., Brown, R., Bhatt, U. S., Euskirchen, E. S., Romanovsky, V. E., Walsh, J. E., Overland, J. E., Wang, M., Corell, R. W., Meier, W. N., Wouters, B., Mernild, S., Mård, J., Pawlak, J., and Olsen, M. S.: Key indicators of Arctic climate change: 1971-2017, Environmental Research Letters, 14, https://doi.org/10.1088/1748-9326/aafc1b, 2019.

Bridgham, S. D., Cadillo-Quiroz, H., Keller, J. K., and Zhuang, Q.: Methane emissions from wetlands: Biogeochemical, microbial, and modeling perspectives from local to global scales, Global Change Biology, 19, 1325–1346, https://doi.org/10.1111/gcb.12131, 2013.

De Boeck, H. J., Dreesen, F. E., Janssens, I. A., and Nijs, I.: Whole-system responses of experimental plant communities to climate extremes imposed in different seasons, New Phytologist, 189, 806–817, https://doi.org/10.1111/j.1469-8137.2010.03515.x, http://www.ncbi.nlm.nih.gov/pubmed/21054412, 2011.

De Lange, W. J., Prinsen, G. F., Hoogewoud, J. C., Veldhuizen, A. A., Verkaik, J., Oude Essink, G. H., Van Walsum, P. E., Delsman, J. R., Hunink, J. C., Massop, H. T. L., and Kroon, T.: An operational, multi-scale, multi-model system for consensus-based, integrated water management and policy analysis: The Netherlands Hydrological Instrument., Environmental Modelling and Software, 59, 98–108, https://doi.org/10.1016/j.envsoft.2014.05.009, http://dx.doi.org/10.1016/j.envsoft.2014.05.009, 2014.

Dorrepaal, E., Aerts, R., Cornelissen, J. H., Van Logtestijn, R. S., and Callaghan, T. V.: Sphagnum modifies climate-change impacts on subarctic vascular bog plants, Functional Ecology, 20, 31–41, https://doi.org/10.1111/j.1365-2435.2006.01076.x, 2006.

Dorrepaal, E., Cornelissen, J. H., and Aerts, R.: Changing leaf litter feedbacks on plant production across contrasting sub-arctic peatland species and growth forms, Oecologia, 151, 251–261, https://doi.org/10.1007/s00442-006-0580-3, 2007.

Dorrepaal, E., Toet, S., Van Logtestijn, R. S., Swart, E., Van De Weg, M. J., Callaghan, T. V., and Aerts, R.: Carbon respiration from subsurface peat accelerated by climate warming in the subarctic, Nature, 460, 616–619, https://doi.org/10.1038/nature08216, http://dx.doi.org/10.1038/nature08216, 2009.

Frolking, S. and Roulet, N. T.: Holocene radiative forcing impact of northern peatland carbon accumulation and methane emissions, Global Change Biology, 13, 1079–1088, https://doi.org/10.1111/j.1365-2486.2007.01339.x, 2007.

https://doi.org/10.5194/gmd-2023-48
Preprint. Discussion started: 29 March 2023

Geurts, J. and Fritz, C.: Paludiculture pilots and experiments with focus on cattail and reed in the Netherlands. Technical, Tech. rep., Radboud University Nijmegen, Nijmegen, https://repository.ubn.ru.nl/handle/2066/192628, 2018.

Graf, M. and Rochefort, L.: Examining the peat-accumulating potential of fen vegetation in the context of fen restoration of harvested peatlands, Ecoscience, 16, 158–166, https://doi.org/10.2980/16-2-3128, 2009.

Granberg, G., Grip, H., Ottosson Löfvenius, M., Sundh, I., Svensson, B. H., and Nilsson, M.: A simple model for simulation of water content, soil frost, and soil temperatures in boreal mixed mires, Water Resources Research, 35, 3771–3782, https://doi.org/10.1029/1999WR900216, 1999.

Günther, A., Huth, V., Jurasinski, G., and Glatzel, S.: The effect of biomass harvesting on greenhouse gas emissions from a rewetted temperate fen, GCB Bioenergy, 7, 1092–1106, https://doi.org/10.1111/gcbb.12214, 2015.

Günther, A., Barthelmes, A., Huth, V., Joosten, H., Jurasinski, G., Koebsch, F., and Couwenberg, J.: Prompt rewetting of drained peatlands reduces climate warming despite methane emissions, Nature Communications, 11, 1644, https://doi.org/10.1038/s41467-020-15499-z, http://www.nature.com/articles/s41467-020-15499-z, 2020.

Harpenslager, S. F., van den Elzen, E., Kox, M. A., Smolders, A. J., Ettwig, K. F., and Lamers, L. P.: Rewetting former agricultural peatlands: Topsoil removal as a prerequisite to avoid strong nutrient and greenhouse gas emissions, Ecological Engineering, 84, 159–168, https://doi.org/10.1016/j.ecoleng.2015.08.002, http://dx.doi.org/10.1016/j.ecoleng.2015.08.002, 2015.

Haxeltine, A., Prentice, I. C., and Creswell, I. D.: A coupled carbon and water flux model to predict vegetation structure, Journal of Vegetation Science, 7, 651–666, https://doi.org/10.2307/3236377, 1996.

Heijmans, M. and Berendse, F.: NUCOM: a dynamic vegetation model for peatlands and tundra including nitrogen cycling and mosses, 2008.

Hendriks, D. M., Van Huissteden, J., Dolman, A. J., and Van Der Molen, M. K.: The full greenhouse gas balance of an abandoned peat meadow, Biogeosciences, 4, 411–424, https://doi.org/10.5194/bg-4-411-2007, 2007.

Hobbie, S. E., Schimel, J. P., Trumbore, S. E., and Randerson, J. R.: Controls over carbon storage and turnover in high-latitude soils, Global Change Biology, 6, 196–210, https://doi.org/10.1046/j.1365-2486.2000.06021.x, 2000.

Huang, S., Titus, S. J., and Wiens, D. P.: Comparison of nonlinear height-diameter functions for major Alberta tree species, Canadian Journal of Forest Research, 22, 1297–1304, https://doi.org/10.1139/x92-172, https://cdnsciencepub.com/doi/10.1139/x92-172http://www.nrcresearchpress.com/doi/10.1139/x92-172, 1992.

Iversen, C. M., Sloan, V. L., Sullivan, P. F., Euskirchen, E. S., Mcguire, A. D., Norby, R. J., Walker, A. P., Warren, J. M., and Wullschleger, S. D.: The unseen iceberg: Plant roots in arctic tundra, New Phytologist, 205, 34–58, https://doi.org/10.1111/nph.13003, http://www.ncbi.nlm.nih.gov/pubmed/25209220https://onlinelibrary.wiley.com/doi/10.1111/nph.13003, 2015.

Kattge, J., Díaz, S., Lavorel, S., Prentice, I. C., Leadley, P., Bönisch, G., Garnier, E., Westoby, M., Reich, P. B., Wright, I. J., Cornelissen, J. H., Violle, C., Harrison, S. P., Van Bodegom, P. M., Reichstein, M., Enquist, B. J., Soudzilovskaia, N. A., Ackerly, D. D., Anand, M., Atkin, O., Bahn, M., Baker, T. R., Baldocchi, D., Bekker, R., Blanco, C. C., Blonder, B., Bond, W. J., Bradstock, R., Bunker, D. E., Casanoves, F., Cavender-Bares, J., Chambers, J. Q., Chapin, F. S., Chave, J., Coomes, D., Cornwell, W. K., Craine, J. M., Dobrin, B. H., Duarte, L., Durka, W., Elser, J., Esser, G., Estiarte, M., Fagan, W. F., Fang, J., Fernández-Méndez, F., Fidelis, A., Finegan, B., Flores, O., Ford, H., Frank, D., Freschet, G. T., Fyllas, N. M., Gallagher, R. V., Green, W. A., Gutierrez, A. G., Hickler, T., Higgins, S. I., Hodgson, J. G., Jalili, A., Jansen, S., Joly, C. A., Kerkhoff, A. J., Kirkup, D., Kitajima, K., Kleyer, M., Klotz, S., Knops, J. M., Kramer, K., Kühn, I., Kurokawa, H., Laughlin, D., Lee, T. D., Leishman, M., Lens, F., Lenz, T., Lewis, S. L., Lloyd, J., Llusià, J., Louault, F., Ma, S., Mahecha, M. D., Manning, P., Massad, T., Medlyn, B. E., Messier, J., Moles, A. T., Müller, S. C., Nadrowski, K., Naeem, S., Niinemets, Ü., Nöllert, S.,

https://doi.org/10.5194/gmd-2023-48
Preprint. Discussion started: 29 March 2023

Nüske, A., Ogaya, R., Oleksyn, J., Onipchenko, V. G., Onoda, Y., Ordoñez, J., Overbeck, G., Ozinga, W. A., Patiño, S., Paula, S., Pausas, J. G., Peñuelas, J., Phillips, O. L., Pillar, V., Poorter, H., Poorter, L., Poschlod, P., Prinzing, A., Proulx, R., Rammig, A., Reinsch, S., Reu, B., Sack, L., Salgado-Negret, B., Sardans, J., Shiodera, S., Shipley, B., Siefert, A., Sosinski, E., Soussana, J. F., Swaine, E., Swenson, N., Thompson, K., Thornton, P., Waldram, M., Weiher, E., White, M., White, S., Wright, S. J., Yguel, B., Zaehle, S., Zanne, A. E., and Wirth, C.: TRY - a global database of plant traits, Global Change Biology, 17, 2905–2935, https://doi.org/10.1111/j.1365-2486.2011.02451.x, 2011.

Kattge, J., Bönisch, G., Díaz, S., Lavorel, S., Prentice, I. C., Leadley, P., Tautenhahn, S., Werner, G. D., Aakala, T., Abedi, M., Acosta, A. T., Adamidis, G. C., Adamson, K., Aiba, M., Albert, C. H., Alcántara, J. M., Alcázar C, C., Aleixo, I., Ali, H., Amiaud, B., Ammer, C., Amoroso, M. M., Anand, M., Anderson, C., Anten, N., Antos, J., Apgaua, D. M. G., Ashman, T. L., Asmara, D. H., Asner, G. P., Aspinwall, M., Atkin, O., Aubin, I., Baastrup-Spohr, L., Bahalkeh, K., Bahn, M., Baker, T., Baker, W. J., Bakker, J. P., Baldocchi, D., Baltzer, J., Banerjee, A., Baranger, A., Barlow, J., Barneche, D. R., Baruch, Z., Bastianelli, D., Battles, J., Bauerle, W., Bauters, M., Bazzato, E., Beckmann, M., Beeckman, H., Beierkuhnlein, C., Bekker, R., Belfry, G., Belluau, M., Beloiu, M., Benavides, R., Benomar, L., Berdugo-Lattke, M. L., Berenguer, E., Bergamin, R., Bergmann, J., Bergmann Carlucci, M., Berner, L., Bernhardt-Römermann, M., Bigler, C., Bjorkman, A. D., Blackman, C., Blanco, C., Blonder, B., Blumenthal, D., Bocanegra-González, K. T., Boeckx, P., Bohlman, S., Böhning-Gaese, K., Boisvert-Marsh, L., Bond, W., Bond-Lamberty, B., Boom, A., Boonman, C. C., Bordin, K., Boughton, E. H., Boukili, V., Bowman, D. M., Bravo, S., Brendel, M. R., Broadley, M. R., Brown, K. A., Bruelheide, H., Brumnich, F., Bruun, H. H., Bruy, D., Buchanan, S. W., Bucher, S. F., Buchmann, N., Buitenwerf, R., Bunker, D. E., Bürger, J., Burrascano, S., Burslem, D. F., Butterfield, B. J., Byun, C., Marques, M., Scalon, M. C., Caccianiga, M., Cadotte, M., Cailleret, M., Camac, J., Camarero, J. J., Campany, C., Campetella, G., Campos, J. A., Cano-Arboleda, L., Canullo, R., Carbognani, M., Carvalho, F., Casanoves, F., Castagneyrol, B., Catford, J. A., Cavender-Bares, J., Cerabolini, B. E., Cervellini, M., Chacón-Madrigal, E., Chapin, K., Chapin, F. S., Chelli, S., Chen, S. C., Chen, A., Cherubini, P., Chianucci, F., Choat, B., Chung, K. S., Chytrý, M., Ciccarelli, D., Coll, L., Collins, C. G., Conti, L., Coomes, D., Cornelissen, J. H., Cornwell, W. K., Corona, P., Coyea, M., Craine, J., Craven, D., Cromsigt, J. P., Csecserits, A., Cufar, K., Cuntz, M., da Silva, A. C., Dahlin, K. M., Dainese, M., Dalke, I., Dalle Fratte, M., Dang-Le, A. T., Danihelka, J., Dannoura, M., Dawson, S., de Beer, A. J., De Frutos, A., De Long, J. R., Dechant, B., Delagrange, S., Delpierre, N., Derroire, G., Dias, A. S., Diaz-Toribio, M. H., Dimitrakopoulos, P. G., Dobrowolski, M., Doktor, D., Dřevojan, P., Dong, N., Dransfield, J., Dressler, S., Duarte, L., Ducouret, E., Dullinger, S., Durka, W., Duursma, R., Dymova, O., E-Vojtkó, A., Eckstein, R. L., Ejtehadi, H., Elser, J., Emilio, T., Engemann, K., Erfanian, M. B., Erfmeier, A., Esquivel-Muelbert, A., Esser, G., Estiarte, M., Domingues, T. F., Fagan, W. F., Fagúndez, J., Falster, D. S., Fan, Y., Fang, J., Farris, E., Fazlioglu, F., Feng, Y., Fernandez-Mendez, F., Ferrara, C., Ferreira, J., Fidelis, A., Finegan, B., Firn, J., Flowers, T. J., Flynn, D. F., Fontana, V., Forey, E., Forgiarini, C., François, L., Frangipani, M., Frank, D., Frenette-Dussault, C., Freschet, G. T., Fry, E. L., Fyllas, N. M., Mazzochini, G. G., Gachet, S., Gallagher, R., Ganade, G., Ganga, F., García-Palacios, P., Gargaglione, V., Garnier, E., Garrido, J. L., de Gasper, A. L., Gea-Izquierdo, G., Gibson, D., Gillison, A. N., Giroldo, A., Glasenhardt, M. C., Gleason, S., Gliesch, M., Goldberg, E., Göldel, B., Gonzalez-Akre, E., Gonzalez-Andujar, J. L., González-Melo, A., González-Robles, A., Graae, B. J., Granda, E., Graves, S., Green, W. A., Gregor, T., Gross, N., Guerin, G. R., Günther, A., Gutiérrez, A. G., Haddock, L., Haines, A., Hall, J., Hambuckers, A., Han, W., Harrison, S. P., Hattingh, W., Hawes, J. E., He, T., He, P., Heberling, J. M., Helm, A., Hempel, S., Hentschel, J., Hérault, B., Hereş, A. M., Herz, K., Heuertz, M., Hickler, T., Hietz, P., Higuchi, P., Hipp, A. L., Hirons, A., Hock, M., Hogan, J. A., Holl, K., Honnay, O., Hornstein, D., Hou, E., Hough-Snee, N., Hovstad, K. A., Ichie, T., Igić, B., Illa, E., Isaac, M., Ishihara, M., Ivanov, L., Ivanova, L., Iversen, C. M., Izquierdo, J., Jackson, R. B., Jackson, B., Jactel, H., Jagodzinski, A. M., Jandt, U., Jansen, S., Jenkins, T., Jentsch, A., Jespersen, J. R. P., Jiang, G. F., Johansen, J. L., Johnson, D., Jokela, E. J., Joly, C. A., Jordan, G. J., Joseph, G. S., Junaedi, D., Junker,

https://doi.org/10.5194/gmd-2023-48
Preprint. Discussion started: 29 March 2023

R. R., Justes, E., Kabzems, R., Kane, J., Kaplan, Z., Kattenborn, T., Kavelenova, L., Kearsley, E., Kempel, A., Kenzo, T., Kerkhoff, A., Khalil, M. I., Kinlock, N. L., Kissling, W. D., Kitajima, K., Kitzberger, T., Kjøller, R., Klein, T., Kleyer, M., Klimešová, J., Klipel, J., Kloeppel, B., Klotz, S., Knops, J. M., Kohyama, T., Koike, F., Kollmann, J., Komac, B., Komatsu, K., König, C., Kraft, N. J., Kramer, K., Kreft, H., Kühn, I., Kumarathunge, D., Kuppler, J., Kurokawa, H., Kurosawa, Y., Kuyah, S., Laclau, J. P., Lafleur, B., Lallai, E., Lamb, E., Lamprecht, A., Larkin, D. J., Laughlin, D., Le Bagousse-Pinguet, Y., le Maire, G., le Roux, P. C., le Roux, E., Lee, T., Lens, F., Lewis, S. L., Lhotsky, B., Li, Y., Li, X., Lichstein, J. W., Liebergesell, M., Lim, J. Y., Lin, Y. S., Linares, J. C., Liu, C., Liu, D., Liu, U., Livingstone, S., Llusià, J., Lohbeck, M., López-García, Á., Lopez-Gonzalez, G., Lososová, Z., Louault, F., Lukács, B. A., Lukeš, P., Luo, Y., Lussu, M., Ma, S., Maciel Rabelo Pereira, C., Mack, M., Maire, V., Mäkelä, A., Mäkinen, H., Malhado, A. C. M., Mallik, A., Manning, P., Manzoni, S., Marchetti, Z., Marchino, L., Marcilio-Silva, V., Marcon, E., Marignani, M., Markesteijn, L., Martin, A., Martínez-Garza, C., Martínez-Vilalta, J., Mašková, T., Mason, K., Mason, N., Massad, T. J., Masse, J., Mayrose, I., McCarthy, J., McCormack, M. L., McCulloh, K., McFadden, I. R., McGill, B. J., McPartland, M. Y., Medeiros, J. S., Medlyn, B., Meerts, P., Mehrabi, Z., Meir, P., Melo, F. P., Mencuccini, M., Meredieu, C., Messier, J., Mészáros, I., Metsaranta, J., Michaletz, S. T., Michelaki, C., Migalina, S., Milla, R., Miller, J. E., Minden, V., Ming, R., Mokany, K., Moles, A. T., Molnár, A., Molofsky, J., Molz, M., Montgomery, R. A., Monty, A., Moravcová, L., Moreno-Martínez, A., Moretti, M., Mori, A. S., Mori, S., Morris, D., Morrison, J., Mucina, L., Mueller, S., Muir, C. D., Müller, S. C., Munoz, F., Myers-Smith, I. H., Myster, R. W., Nagano, M., Naidu, S., Narayanan, A., Natesan, B., Negoita, L., Nelson, A. S., Neuschulz, E. L., Ni, J., Niedrist, G., Nieto, J., Niinemets, Ü., Nolan, R., Nottebrock, H., Nouvellon, Y., Novakovskiy, A., Nystuen, K. O., O'Grady, A., O'Hara, K., O'Reilly-Nugent, A., Oakley, S., Oberhuber, W., Ohtsuka, T., Oliveira, R., Öllerer, K., Olson, M. E., Onipchenko, V., Onoda, Y., Onstein, R. E., Ordonez, J. C., Osada, N., Ostonen, I., Ottaviani, G., Otto, S., Overbeck, G. E., Ozinga, W. A., Pahl, A. T., Paine, C. E., Pakeman, R. J., Papageorgiou, A. C., Parfionova, E., Pärtel, M., Patacca, M., Paula, S., Paule, J., Pauli, H., Pausas, J. G., Peco, B., Penuelas, J., Perea, A., Peri, P. L., Petisco-Souza, A. C., Petraglia, A., Petritan, A. M., Phillips, O. L., Pierce, S., Pillar, V. D., Pisek, J., Pomogaybin, A., Poorter, H., Portsmuth, A., Poschlod, P., Potvin, C., Pounds, D., Powell, A. S., Power, S. A., Prinzing, A., Puglielli, G., Pyšek, P., Raevel, V., Rammig, A., Ransijn, J., Ray, C. A., Reich, P. B., Reichstein, M., Reid, D. E., Réjou-Méchain, M., de Dios, V. R., Ribeiro, S., Richardson, S., Riibak, K., Rillig, M. C., Riviera, F., Robert, E. M., Roberts, S., Robroek, B., Roddy, A., Rodrigues, A. V., Rogers, A., Rollinson, E., Rolo, V., Römermann, C., Ronzhina, D., Roscher, C., Rosell, J. A., Rosenfield, M. F., Rossi, C., Roy, D. B., Royer-Tardif, S., Rüger, N., Ruiz-Peinado, R., Rumpf, S. B., Rusch, G. M., Ryo, M., Sack, L., Saldaña, A., Salgado-Negret, B., Salguero-Gomez, R., Santa-Regina, I., Santacruz-García, A. C., Santos, J., Sardans, J., Schamp, B., Scherer-Lorenzen, M., Schleuning, M., Schmid, B., Schmidt, M., Schmitt, S., Schneider, J. V., Schowanek, S. D., Schrader, J., Schrodt, F., Schuldt, B., Schurr, F., Selaya Garvizu, G., Semchenko, M., Seymour, C., Sfair, J. C., Sharpe, J. M., Sheppard, C. S., Sheremetiev, S., Shiodera, S., Shipley, B., Shovon, T. A., Siebenkäs, A., Sierra, C., Silva, V., Silva, M., Sitzia, T., Sjöman, H., Slot, M., Smith, N. G., Sodhi, D., Soltis, P., Soltis, D., Somers, B., Sonnier, G., Sørensen, M. V., Sosinski, E. E., Soudzilovskaia, N. A., Souza, A. F., Spasojevic, M., Sperandii, M. G., Stan, A. B., Stegen, J., Steinbauer, K., Stephan, J. G., Sterck, F., Stojanovic, D. B., Strydom, T., Suarez, M. L., Svenning, J. C., Svitková, I., Svitok, M., Svoboda, M., Swaine, E., Swenson, N., Tabarelli, M., Takagi, K., Tappeiner, U., Tarifa, R., Tauugourdeau, S., Tavsanoglu, C., te Beest, M., Tedersoo, L., Thiffault, N., Thom, D., Thomas, E., Thompson, K., Thornton, P. E., Thuiller, W., Tichý, L., Tissue, D., Tjoelker, M. G., Tng, D. Y. P., Tobias, J., Török, P., Tarin, T., Torres-Ruiz, J. M., Tóthmérész, B., Treurnicht, M., Trivellone, V., Trolliet, F., Trotsiuk, V., Tsakalos, J. L., Tsiripidis, I., Tysklind, N., Umehara, T., Usoltsev, V., Vadeboncoeur, M., Vaezi, J., Valladares, F., Vamosi, J., van Bodegom, P. M., van Breugel, M., Van Cleemput, E., van de Weg, M., van der Merwe, S., van der Plas, F., van der Sande, M. T., van Kleunen, M., Van Meerbeek, K., Vanderwel, M., Vanselow, K. A., Vårhammar, A., Varone, L., Vasquez Valderrama, M. Y., Vassilev, K., Vellend, M., Veneklaas, E. J., Verbeeck, H., Verheyen, K., Vibrans, A., Vieira, I., Villacís, J., Violle, C., Vivek, P., Wagner, K., Waldram,

https://doi.org/10.5194/gmd-2023-48
Preprint. Discussion started: 29 March 2023

M., Waldron, A., Walker, A. P., Waller, M., Walther, G., Wang, H., Wang, F., Wang, W., Watkins, H., Watkins, J., Weber, U., Weedon, J. T., Wei, L., Weigelt, P., Weiher, E., Wells, A. W., Wellstein, C., Wenk, E., Westoby, M., Westwood, A., White, P. J., Whitten, M., Williams, M., Winkler, D. E., Winter, K., Womack, C., Wright, I. J., Wright, S. J., Wright, J., Pinho, B. X., Ximenes, F., Yamada, T., Yamaji, K., Yanai, R., Yankov, N., Yguel, B., Zanini, K. J., Zanne, A. E., Zelený, D., Zhao, Y. P., Zheng, J., Zheng, J., Ziemińska, K., Zirbel, C. R., Zizka, G., Zo-Bi, I. C., Zotz, G., and Wirth, C.: TRY plant trait database – enhanced coverage and open access, Global Change Biology, 26, 119–188, https://doi.org/10.1111/gcb.14904, 2020.

Knox, S. H., Sturtevant, C., Matthes, J. H., Koteen, L., Verfaillie, J., and Baldocchi, D.: Agricultural peatland restoration: Effects of land-use change on greenhouse gas (CO2 and CH4) fluxes in the Sacramento-San Joaquin Delta, Global Change Biology, 21, 750–765, https://doi.org/10.1111/gcb.12745, 2015.

Lafleur, P. M., Roulet, N. T., Bubier, J. L., Frolking, S., and Moore, T. R.: Interannual variability in the peatland-atmosphere carbon dioxide exchange at an ombrotrophic bog, Global Biogeochemical Cycles, 17, 1–14, https://doi.org/10.1029/2002gb001983, 2003.

Laine, A. M., Korrensalo, A., and Tuittila, E. S.: Plant functional traits play the second fiddle to plant functional types in explaining peatland CO2 and CH4 gas exchange, Science of the Total Environment, 834, 155 352, https://doi.org/10.1016/j.scitotenv.2022.155352, https://doi.org/10.1016/j.scitotenv.2022.155352, 2022.

Li, T., Raivonen, M., Alekseychik, P., Aurela, M., Lohila, A., Zheng, X., Zhang, Q., Wang, G., Mammarella, I., Rinne, J., Yu, L., Xie, B., Vesala, T., and Zhang, W.: Importance of vegetation classes in modeling CH4 emissions from boreal and subarctic wetlands in Finland, Science of the Total Environment, 572, 1111–1122, https://doi.org/10.1016/j.scitotenv.2016.08.020, http://dx.doi.org/10.1016/j.scitotenv.2016.08.020, 2016.

Lippmann, T. J. R. and van Huissteden, J.: Peatland-VU-NUCOM (PVN 1.0): A peatland GHG emissions model using dynamic plant functional types, https://doi.org/https://doi.org/10.5281/zenodo.7701698, https://zenodo.org/record/7701698, 2023.

Littleton, E. W., Harper, A. B., Vaughan, N. E., Oliver, R. J., Duran-Rojas, M. C., and Lenton, T. M.: JULES-BE: Representation of bioenergy crops and harvesting in the Joint UK Land Environment Simulator vn5.1, Geoscientific Model Development, 13, 1123–1136, https://doi.org/10.5194/gmd-13-1123-2020, https://gmd.copernicus.org/articles/13/1123/2020/, 2020.

Loisel, J., Gallego-Sala, A. V., Amesbury, M. J., Magnan, G., Anshari, G., Beilman, D. W., Benavides, J. C., Blewett, J., Camill, P., Charman, D. J., Chawchai, S., Hedgpeth, A., Kleinen, T., Korhola, A., Large, D., Mansilla, C. A., Müller, J., van Bellen, S., West, J. B., Yu, Z., Bubier, J. L., Garneau, M., Moore, T., Sannel, A. B., Page, S., Väliranta, M., Bechtold, M., Brovkin, V., Cole, L. E., Chanton, J. P., Christensen, T. R., Davies, M. A., De Vleeschouwer, F., Finkelstein, S. A., Frolking, S., Gałka, M., Gandois, L., Girkin, N., Harris, L. I., Heinemeyer, A., Hoyt, A. M., Jones, M. C., Joos, F., Juutinen, S., Kaiser, K., Lacourse, T., Lamentowicz, M., Larmola, T., Leifeld, J., Lohila, A., Milner, A. M., Minkkinen, K., Moss, P., Naafs, B. D., Nichols, J., O'Donnell, J., Payne, R., Philben, M., Piilo, S., Quillet, A., Ratnayake, A. S., Roland, T. P., Sjögersten, S., Sonnentag, O., Swindles, G. T., Swinnen, W., Talbot, J., Treat, C., Valach, A. C., and Wu, J.: Expert assessment of future vulnerability of the global peatland carbon sink, Nature Climate Change, 11, 70–77, https://doi.org/10.1038/s41558-020-00944-0, 2021.

Masson-Delmotte, V., Zhai, P., Pirani, A., Connors, S. L., Péan, C., Berger, S., Caud, N., Chen, Y., Goldfarb, L., Gomis, M. I., Huang, M., Leitzell, K., Lonnoy, E., Matthews, J. B. R., Maycock, T. K., Waterfield, T., Yelekçi, O., Yu, R., and Zhou, B., eds.: Climate Change 2021: The Physical Science Basis. Contribution of Working Group I to the Sixth Assessment Report of the Intergovernmental Panel on Climate Change, vol. In Press, Cambridge University Press, Cambridge, United Kingdom and New York, NY, USA, https://doi.org/10.1017/9781009157896, 2021.

https://doi.org/10.5194/gmd-2023-48
Preprint. Discussion started: 29 March 2023

Mazzola, V., Perks, M. P., Smith, J., Yeluripati, J., and Xenakis, G.: Assessing soil carbon dioxide and methane fluxes from a Scots pine raised bog-edge-woodland, Journal of Environmental Management, 302, 114 061, https://doi.org/10.1016/j.jenvman.2021.114061, https://doi.org/10.1016/j.jenvman.2021.114061, 2022.

Melillo, J. M., Steudler, P. A., Aber, J. D., Newkirk, K., Lux, H., Bowles, F. P., Catricala, C., Magill, A., Ahrens, T., and Morrisseau, S.: Soil warming and carbon-cycle feedbacks to the climate system, Science, 298, 2173–2176, https://doi.org/10.1126/science.1074153, 2002.

Melton, J. R., Wania, R., Hodson, E. L., Poulter, B., Ringeval, B., Spahni, R., Bohn, T., Avis, C. A., Beerling, D. J., Chen, G., Eliseev, A. V., Denisov, S. N., Hopcroft, P. O., Lettenmaier, D. P., Riley, W. J., Singarayer, J. S., Subin, Z. M., Tian, H., Zürcher, S., Brovkin, V., van Bodegom, P. M., Kleinen, T., Yu, Z. C., and Kaplan, J. O.: Present state of global wetland extent and wetland methane modelling: conclusions from a model inter-comparison project (WETCHIMP), Biogeosciences, 10, 753–788, https://doi.org/10.5194/bg-10-753-2013, https://bg.copernicus.org/articles/10/753/2013/, 2013.

Metzger, C., Jansson, P. E., Lohila, A., Aurela, M., Eickenscheidt, T., Belelli-Marchesini, L., Dinsmore, K. J., Drewer, J., Van Huissteden, J., and Drösler, M.: CO2 fluxes and ecosystem dynamics at five European treeless peatlands-merging data and process oriented modeling, Biogeosciences, 12, 125–146, https://doi.org/10.5194/bg-12-125-2015, http://www.biogeosciences.net/12/125/2015/https://bg.copernicus.org/articles/12/125/2015/, 2015.

Mi, Y., Van Huissteden, J., Parmentier, F. J. W., Gallagher, A., Budishchev, A., Berridge, C. T., and Dolman, A. J.: Improving a plot-scale methane emission model and its performance at a northeastern Siberian tundra site, Biogeosciences, 11, 3985–3999, https://doi.org/10.5194/bg-11-3985-2014, 2014.

Moore, T. R., Bubier, J. L., and Bledzki, L.: Litter decomposition in temperate peatland ecosystems: The effect of substrate and site, Ecosystems, 10, 949–963, https://doi.org/10.1007/s10021-007-9064-5, http://link.springer.com/10.1007/s10021-007-9064-5, 2007.

Morin, T. H., Bohrer, G., Frasson, R. P., Naor-Azreli, L., Mesi, S., Stefanik, K. C., and Schäfer, K. V.: Environmental drivers of methane fluxes from an urban temperate wetland park, Journal of Geophysical Research: Biogeosciences, 119, 2188–2208, https://doi.org/10.1002/2014JG002750, 2014a.

Morin, T. H., Bohrer, G., Naor-Azrieli, L., Mesi, S., Kenny, W. T., Mitsch, W. J., and Schäfer, K. V. R.: The seasonal and diurnal dynamics of methane flux at a created urban wetland, Ecological Engineering, 72, 74–83, https://doi.org/10.1016/j.ecoleng.2014.02.002, http://dx.doi.org/10.1016/j.ecoleng.2014.02.002, 2014b.

Morin, T. H., Bohrer, G., Stefanik, K. C., Rey-Sanchez, A. C., Matheny, A. M., and Mitsch, W. J.: Combining eddy-covariance and chamber measurements to determine the methane budget from a small, heterogeneous urban floodplain wetland park, Agricultural and Forest Meteorology, 237-238, 160–170, https://doi.org/10.1016/j.agrformet.2017.01.022, http://dx.doi.org/10.1016/j.agrformet.2017.01.022, 2017.

Pangala, S. R., Moore, S., Hornibrook, E. R., and Gauci, V.: Trees are major conduits for methane egress from tropical forested wetlands, New Phytologist, 197, 524–531, https://doi.org/10.1111/nph.12031, 2013.

Pavelka, M., Acosta, M., Kiese, R., Altimir, N., Brümmer, C., Crill, P., Darenova, E., Fuß, R., Gielen, B., Graf, A., Klemedtsson, L., Lohila, A., Longdoz, B., Lindroth, A., Nilsson, M., Jiménez, S. M., Merbold, L., Montagnani, L., Peichl, M., Pihlatie, M., Pumpanen, J., Ortiz, P. S., Silvennoinen, H., Skiba, U., Vestin, P., Weslien, P., Janous, D., and Kutsch, W.: Standardisation of chamber technique for CO 2 , N 2 O and CH 4 fluxes measurements from terrestrial ecosystems, International Agrophysics, 32, 569–587, https://doi.org/10.1515/intag-2017-0045, 2018.

Saleska, S. R., Shaw, M. R., Fischer, M. L., Dunne, J. A., Still, C. J., Holman, M. L., and Harte, J.: Plant community composition mediates both large transient decline and predicted long-term recovery of soil carbon under climate warming, Global Biogeochemical Cycles, 16, 3–1–3–18, https://doi.org/10.1029/2001gb001573, 2002.

https://doi.org/10.5194/gmd-2023-48
Preprint. Discussion started: 29 March 2023

Saunois, M., R. Stavert, A., Poulter, B., Bousquet, P., G. Canadell, J., B. Jackson, R., A. Raymond, P., J. Dlugokencky, E., Houweling, S., K. Patra, P., Ciais, P., K. Arora, V., Bastviken, D., Bergamaschi, P., R. Blake, D., Brailsford, G., Bruhwiler, L., M. Carlson, K., Carrol, M., Castaldi, S., Chandra, N., Crevoisier, C., M. Crill, P., Covey, K., L. Curry, C., Etiope, G., Frankenberg, C., Gedney, N., I. Hegglin, M., Höglund-Isaksson, L., Hugelius, G., Ishizawa, M., Ito, A., Janssens-Maenhout, G., M. Jensen, K., Joos, F., Kleinen, T., B. Krummel, P., L. Langenfelds, R., G. Laruelle, G., Liu, L., MacHida, T., Maksyutov, S., C. McDonald, K., McNorton, J., A. Miller, P., R. Melton, J., Morino, I., Müller, J., Murguia-Flores, F., Naik, V., Niwa, Y., Noce, S., O'Doherty, S., J. Parker, R., Peng, C., Peng, S., P. Peters, G., Prigent, C., Prinn, R., Ramonet, M., Regnier, P., J. Riley, W., A. Rosentreter, J., Segers, A., J. Simpson, I., Shi, H., J. Smith, S., Paul Steele, L., F. Thornton, B., Tian, H., Tohjima, Y., N. Tubiello, F., Tsuruta, A., Viovy, N., Voulgarakis, A., S. Weber, T., Van Weele, M., R. Van Der Werf, G., F. Weiss, R., Worthy, D., Wunch, D., Yin, Y., Yoshida, Y., Zhang, W., Zhang, Z., Zhao, Y., Zheng, B., Zhu, Q., Zhu, Q., and Zhuang, Q.: The global methane budget 2000-2017, Earth System Science Data, 12, 1561–1623, https://doi.org/10.5194/essd-12-1561-2020, 2020.

Smith, B., Prentice, I. C., and Sykes, M. T.: Representation of vegetation dynamics in the modelling of terrestrial ecosystems: comparing two contrasting approaches within European climate space, Global Ecology and Biogeography, 10, 621–637, https://doi.org/10.1046/j.1466-822x.2001.t01-1-00256.x, 2001.

Spahni, R., Wania, R., Neef, L., Van Weele, M., Pison, I., Bousquet, P., Frankenberg, C., Foster, P. N., Joos, F., Prentice, I. C., and Van Velthoven, P.: Constraining global methane emissions and uptake by ecosystems, Biogeosciences, 8, 1643–1665, https://doi.org/10.5194/bg-8-1643-2011, 2011.

Speckman, H. N., Frank, J. M., Bradford, J. B., Miles, B. L., Massman, W. J., Parton, W. J., and Ryan, M. G.: Forest ecosystem respiration estimated from eddy covariance and chamber measurements under high turbulence and substantial tree mortality from bark beetles, Global Change Biology, 21, 708–721, https://doi.org/10.1111/gcb.12731, 2015.

Ström, L., Mastepanov, M., and Christensen, T. R.: Species-specific effects of vascular plants on carbon turnover and methane emissions from wetlands, Biogeochemistry, 75, 65–82, https://doi.org/10.1007/s10533-004-6124-1, https://doi.org/10.1007/s10533-004-6124-1http://link.springer.com/10.1007/s10533-004-6124-1, 2005.

Tiemeyer, B., Albiac Borraz, E., Augustin, J., Bechtold, M., Beetz, S., Beyer, C., Drosler, M., Ebli, M., Eickenscheidt, T., Fiedler, S., Forster, C., Freibauer, A., Giebels, M., Glatzel, S., Heinichen, J., Hoffmann, M., Hoper, H., Jurasinski, G., Leiber-Sauheitl, K., Peichl-Brak, M., Rosskopf, N., Sommer, M., and Zeitz, J.: High emissions of greenhouse gases from grasslands on peat and other organic soils, Global Change Biology, 22, 4134–4149, https://doi.org/10.1111/gcb.13303, 2016.

Toet, S., Cornelissen, J. H., Aerts, R., Van Logtestijn, R. S., De Beus, M., and Stoevelaar, R.: Moss responses to elevated CO2 and variation in hydrology in a temperate lowland peatland, Plant Ecology, 182, 27–40, https://doi.org/10.1007/s11258-005-9029-8, 2006.

Van den Hoof, C., Hanert, E., and Vidale, P. L.: Simulating dynamic crop growth with an adapted land surface model - JULES-SUCROS: Model development and validation, Agricultural and Forest Meteorology, 151, 137–153, https://doi.org/10.1016/j.agrformet.2010.09.011, https://linkinghub.elsevier.com/retrieve/pii/S0168192310002571, 2011.

van Geel, B., Bos, J. M., and Pals, J. P.: Archaeological and palaeoecological aspects of a medieval house terp in a reclaimed raiseg bog area in North Holland, Ber. Rijksd. Oudheidkd. Bodemonderz, 33, 419–444, 1983.

van Huissteden, J., van den Bos, R., and Marticorena Alvarez, I.: Modelling the effect of water-table management on CO2 and CH4 fluxes from peat soils, Geologie en Mijnbouw/Netherlands Journal of Geosciences, 85, 3–18, https://doi.org/10.1017/S0016774600021399, 2006.

van Huissteden, J., Petrescu, a. M. R., Hendriks, D. M. D., and Rebel, K. T.: Sensitivity analysis of a wetland methane emission model based on temperate and Arctic wetland sites, Biogeosciences, 6, 9083–9126, https://doi.org/10.5194/bgd-6-9083-2009, 2009.

https://doi.org/10.5194/gmd-2023-48
Preprint. Discussion started: 29 March 2023

Walter, B. P., Heimann, M., and Matthews, E.: Modeling modern methane emissions from natural wetlands 2. Interannual variations 1982-1993, Journal of Geophysical Research Atmospheres, 106, 34 207–34 219, https://doi.org/10.1029/2001JD900164, 2001.

Wania, R., Ross, I., and Prentice, I. C.: Implementation and evaluation of a new methane model within a dynamic global vegetation model: LPJ-WHyMe v1.3.1, Geoscientific Model Development, 3, 565–584, https://doi.org/10.5194/gmd-3-565-2010, 2010.

Wania, R., Melton, J. R., Hodson, E. L., Poulter, B., Ringeval, B., Spahni, R., Bohn, T., Avis, C. A., Chen, G., Eliseev, A. V., Hopcroft, P. O., Riley, W. J., Subin, Z. M., Tian, H., Van Bodegom, P. M., Kleinen, T., Yu, Z. C., Singarayer, J. S., Zürcher, S., Lettenmaier, D. P., Beerling, D. J., Denisov, S. N., Prigent, C., Papa, F., and Kaplan, J. O.: Present state of global wetland extent and wetland methane modelling: Methodology of a model inter-comparison project (WETCHIMP), Geoscientific Model Development, 6, 617–641, https://doi.org/10.5194/gmd-6-617-2013, 2013.

WGI, I. A.: Climate Change 2021 The Physical Science Basis WGI, vol. 34, 2021.

Wu, Y. and Blodau, C.: PEATBOG: a biogeochemical model for analyzing coupled carbon and nitrogen dynamics in northern peatlands, Geoscientific Model Development, 6, 1173–1207, https://doi.org/10.5194/gmd-6-1173-2013, https://gmd.copernicus.org/articles/6/1173/2013/, 2013.

Wu, Y., Verseghy, D. L., and Melton, J. R.: Integrating peatlands into the coupled Canadian Land Surface Scheme (CLASS) v3.6 and the Canadian Terrestrial Ecosystem Model (CTEM) v2.0, Geoscientific Model Development, 9, 2639–2663, https://doi.org/10.5194/gmd-9-2639-2016, https://gmd.copernicus.org/articles/9/2639/2016/, 2016.

Wullschleger, S. D., Epstein, H. E., Box, E. O., Euskirchen, E. S., Goswami, S., Iversen, C. M., Kattge, J., Norby, R. J., Van Bodegom, P. M., and Xu, X.: Plant functional types in Earth system models: Past experiences and future directions for application of dynamic vegetation models in high-latitude ecosystems, Annals of Botany, 114, 1–16, https://doi.org/10.1093/aob/mcu077, https://academic.oup.com/aob/article-lookup/doi/10.1093/aob/mcu077, 2014.

Yu, Z., Loisel, J., Brosseau, D. P., Beilman, D. W., and Hunt, S. J.: Global peatland dynamics since the Last Glacial Maximum, Geophysical Research Letters, 37, 1–5, https://doi.org/10.1029/2010GL043584, 2010.

Zuo, Z. Y. and Xiao, D.: Linking global to regional climate change, in: Climate Change Research, edited by Masson-Delmotte, V., Zhai, P., Pirani, A., Connors, S. L., Péan, C., Berger, S., Caud, N., Chen, Y., Goldfarb, L., Gomis, M. I., Huang, M., Leitzell, K., Lonnoy, E., Matthews, J. B. R., Maycock, T. K., Waterfield, T., Yelekçi, O., Yu, R., and Zhou, B., vol. 17, pp. 705–712, Cambridge University Press, Cambridge, United Kingdom and New York, NY, USA, https://doi.org/10.12006/j.issn.1673-1719.2021.176, https://www.ipcc.ch/, 2021.